SLAC-PUB-3245
October 1983
(T/E)

LATEST RESULTS FROM THE MARK II AT PEP*

NIGEL LOCKYER
Stanford Linear Accelerator Center
Stanford University, Stanford, California 94305

ABSTRACT

We present single photon annihilation results from the MARK II detector at PEP based on $\sim$ 100 pb^{-1} of integrated luminosity taken at a center of mass energy $\sqrt{s}$ = 29 GeV. A study of inclusive leptons for momenta $\geq$ 2 GeV/c yield the average semileptonic branching ratios of bottom (b) and charm (c) quarks and information about the b fragmentation function. A measurement of the bottom hadron lifetime is presented based on a study of the prompt lepton impact parameters. In addition we report on a precise measurement of the tau lifetime and an updated D° lifetime. We also present a search for supersymmetric electrons, weak neutral current couplings from leptons and bottom particles and evidence for K*'s at PEP.

---

* Work supported by the Department of Energy, contract DE-AC03-76SF00515.

Presented at the 11th SLAC Summer Institute on Particle Physics
Stanford, California, July 18-29, 1983

1. Introduction

The MARK II group,[1] has investigated several interesting physics topics in e^+e^- annihilation during the last year. Many of the results to be discussed here were made possible by the excellent luminosity and reliable operating conditions of the PEP storage ring since January 1983. At that time a new "mini-beta" scheme (positioning of the final focusing quadrupoles $\sim$ 7 m from the intersection point) enabled a very successful configuration which produced low backgrounds (trigger rate $\sim$ 2 Hz) and a high average luminosity of $\sim$ 1 pb^{-1}/day.[2] By June, we had logged $\sim$ 150 pb^{-1} and processed about two-thirds of that. Another important factor in our physics program was the continued successful operation of a high spatial resolution cylindrical drift chamber, called the MARK II vertex[3] detector, located between the beryllium beam pipe and the main drift chamber. An isometric view of the MARK II detector is shown in Fig. 1 and a closeup of the vertex detector is shown in Fig. 2.

The vertex detector is 120 cm in length, has seven axial layers of drift cells and an average spatial resolution in hadronic events of 110 μ/layer. Tracks are extrapolated to the intersection point with an accuracy of $\sigma_T(\mu) = \sqrt{110^2 + [95/p\,(\mathrm{GeV/c})]^2}$ in the plane perpendicular to the beams, the second term arising from multiple scattering in the 0.6% radiation length (X_0) thick beam pipe. The vertex detector is important for lifetime measurements, reducing the cosmic trigger rate, increasing charged particle tracking acceptance and improving our momentum resolution. When used with the main tracking chamber we obtained a momentum resolution of $\Delta p/p = \sqrt{(0.02)^2 + (0.0095p)^2}$ (p in GeV/c) for tracks constrained to the beam intersection point.

The MARK II solenoid developed a short between the inner and outer coils in January (1982) and we have been operating since then at half field, 0.24T by powering only the outer coil. Fortunately the improved track resolution provided by the vertex detector has nearly cancelled the decrease to the momentum resolution from the lower magnetic field.

The following discussion will be limited to the most recent results from single photon annihilation. For information on recent work not covered here, see Ref. 4.

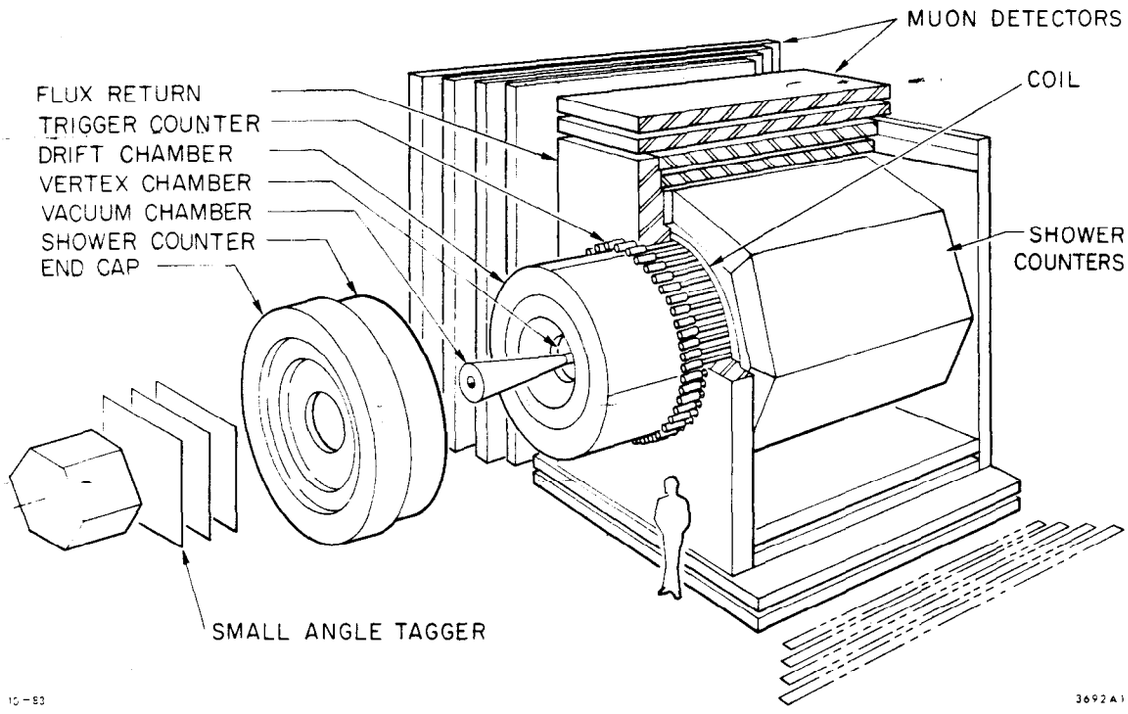

Fig. 1. Isometric view of the MARK II detector.

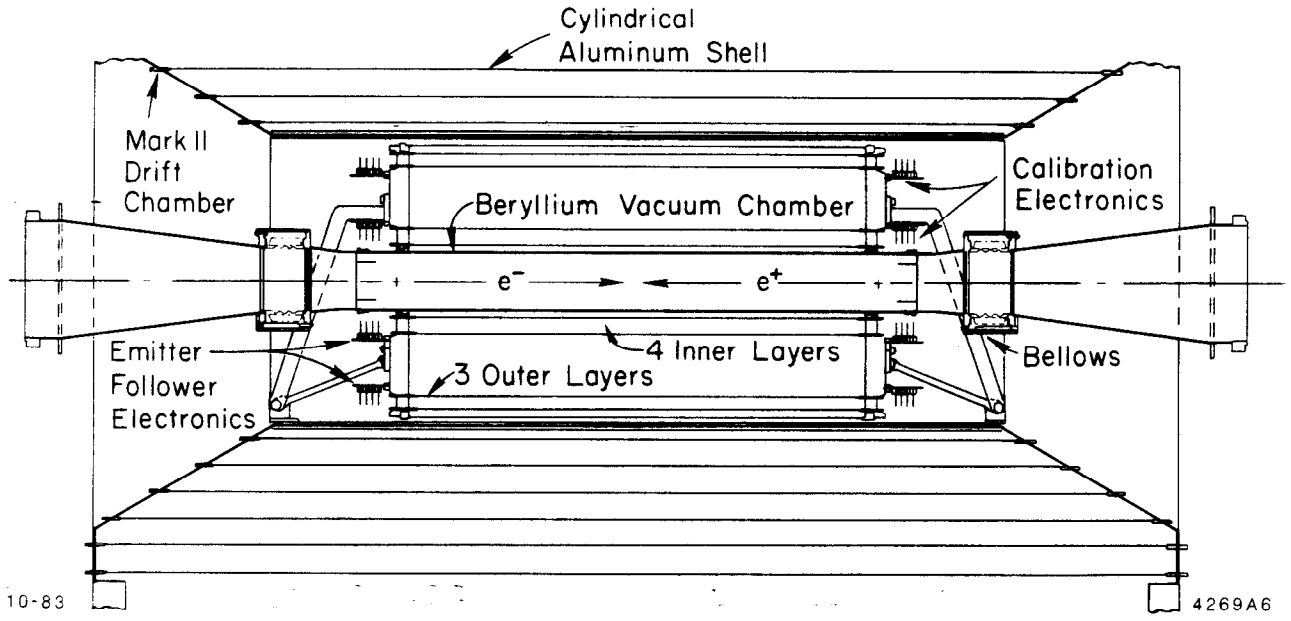

Fig. 2. Cross-section of the vertex detector as installed in the MARK II detector.

2. Inclusive Leptons

The study of prompt leptons in hadronic events produced in high energy e^+e^- annihilation gives information on (c) charm or (b) bottom quarks. In particular the production rates of these leptons depend on the weak semileptonic branching ratios. The momentum spectra of the leptons derive from the parent hadron momentum spectra and this provides information on the quark fragmentation functions. The c and b quarks are expected to pass a larger fraction of their momentum to the hadron containing the heavy quark, contrary to the case with the lighter quarks.[5] Experimental evidence seems to support this point of view for both b and c quarks.[1,6–7] The first experimental information on b quark fragmentation was reported by the MARK II group based on a study of inclusive electrons.[8] Here we report on electrons and muons with a slightly more refined analysis than Ref. 8.

We take advantage in this analysis of the higher mass of the b quark relative to the c quark. This leads to a harder p_T, transverse momentum with respect to the event thrust axis, spectrum of leptons from b decay relative to c decay.[9] After accounting for background we perform a maximum likelihood fit to the lepton populations in p, p_T space. The signal is assumed to come from 3 sources: (i) bottom decays in $b\bar{b}$ events (b primary); (ii) charm decays in $b\bar{b}$ events (c secondary); and (iii) charm decays in $c\bar{c}$ events (c primary). We use a Feynman-Field hadronization model[10] with gluon radiation as incorporated by Ali, et al.,[11] to represent the above processes. The lepton spectra used in the Monte Carlo agree with those of DELCO[12] (charm) and CLEO/CUSB[13] (bottom) experiments.

We have parametrized the b quark fragmentation function D_b^H into hadron H by

$$D_b^H(z) = \frac{A}{z\left[1 - \frac{1}{z} - \frac{\epsilon_b}{(1-z)}\right]^2} \tag{1}$$

where z is E_{hadron}/E_b, A is a normalization factor, and ϵ_b is a parameter. It has been shown that Eq. (1), with $\epsilon_c \simeq .25$ represents the measured charmed meson momentum spectra.[14,15] We have fit for 3 quantities; B_ℓ(b) and B_ℓ(c), the average semileptonic branching ratios in b and c quark decay, and ϵ_b, in Eq. (1). Because of the lepton tag, the average semileptonic branching ratios are averages over all weakly decaying particles, weighted by their relative populations. Furthermore we assume

the production of charm and bottom quark pairs follows from the square of the quark charges when determining B_ℓ(b) and B_ℓ(c). We assume the B_ℓ(c) from contributions (ii) and (iii) is the same and that bottom always decays into charm.

The branching ratios and ϵ parameter values obtained from the fit are given in Table I. The B_ℓ(b) agree well with those obtained at CESR and B_ℓ(c) agree with other PEP/PETRA experiments.[16] The $\langle z \rangle_b \sim$ .75-.80 is indicating a hard b fragmentation in good agreement with other results. The form of the fragmentation function used is shown in Fig. 3.

From this analysis it is interesting to estimate the composition of the signal in terms of the relative fractions of b's, c's, $b \to c \to \ell$, and background. This is shown graphically in Figs. 4 and 5. The ability to select an enriched sample of $b\bar{b}$ events with a p_T cut of greater than one is evident. This will be discussed in more detail in the b lifetime section.

The background to the prompt electrons comes primarily from pions showering in the lead-liquid argon (LA) electromagnetic calorimeter and the overlap associated with photons or other particles within a jet. The algorithm for finding electrons in a strip geometry calorimeter and the technique for determining the misidentification probability is described in detail in Ref. 17. We identify electrons over 65% of 4π with an efficiency

Table I
Branching ratios and fragmentation results

	Electron Results	Muon Results
$B(b)$	$13.5 \pm 2.6 \pm 2.0$	$12.6 \pm 5.2 \pm 3.0$
$B(c)$	$6.6 \pm 1.4 \pm 2.8$	$8.3 \pm 1.3 \pm 1.8$
ϵ_b	$0.015 \begin{smallmatrix} + 0.022 \\ - 0.011 \end{smallmatrix} \begin{smallmatrix} + 0.023 \\ - 0.011 \end{smallmatrix}$	$0.042 \begin{smallmatrix} + 0.218 \\ - 0.041 \end{smallmatrix} \begin{smallmatrix} + 0.120 \\ - 0.035 \end{smallmatrix}$
$\langle z \rangle_b$	$0.79 \pm 0.06 \pm 0.06$	$0.73 \pm 0.15 \pm 0.10$

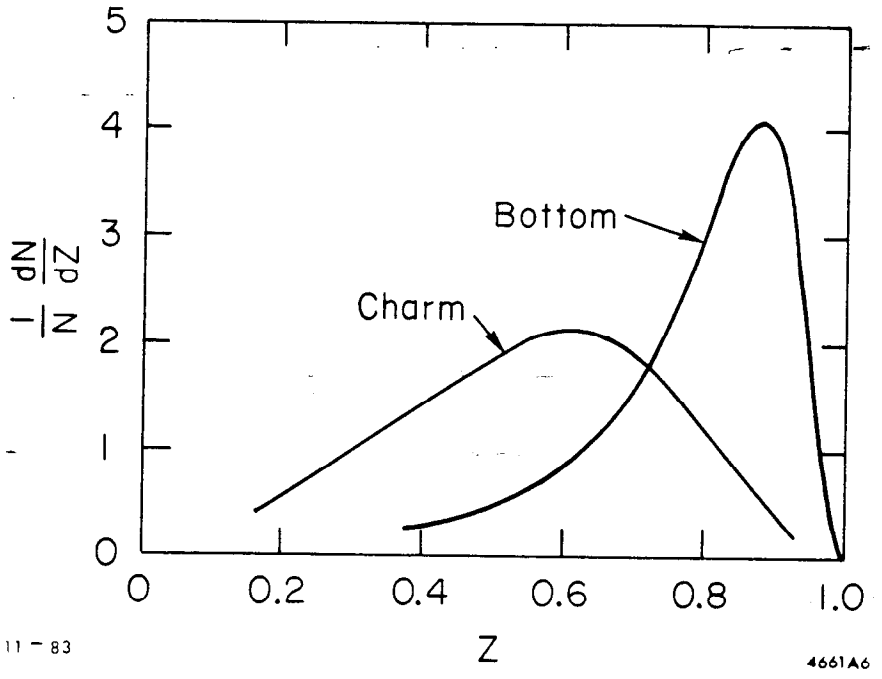

Fig. 3. Comparison of charm and bottom fragmentation functions. Solid curves are results of our fits. From left to right $\epsilon_c = 0.25$, and $\epsilon_b = 0.015$.

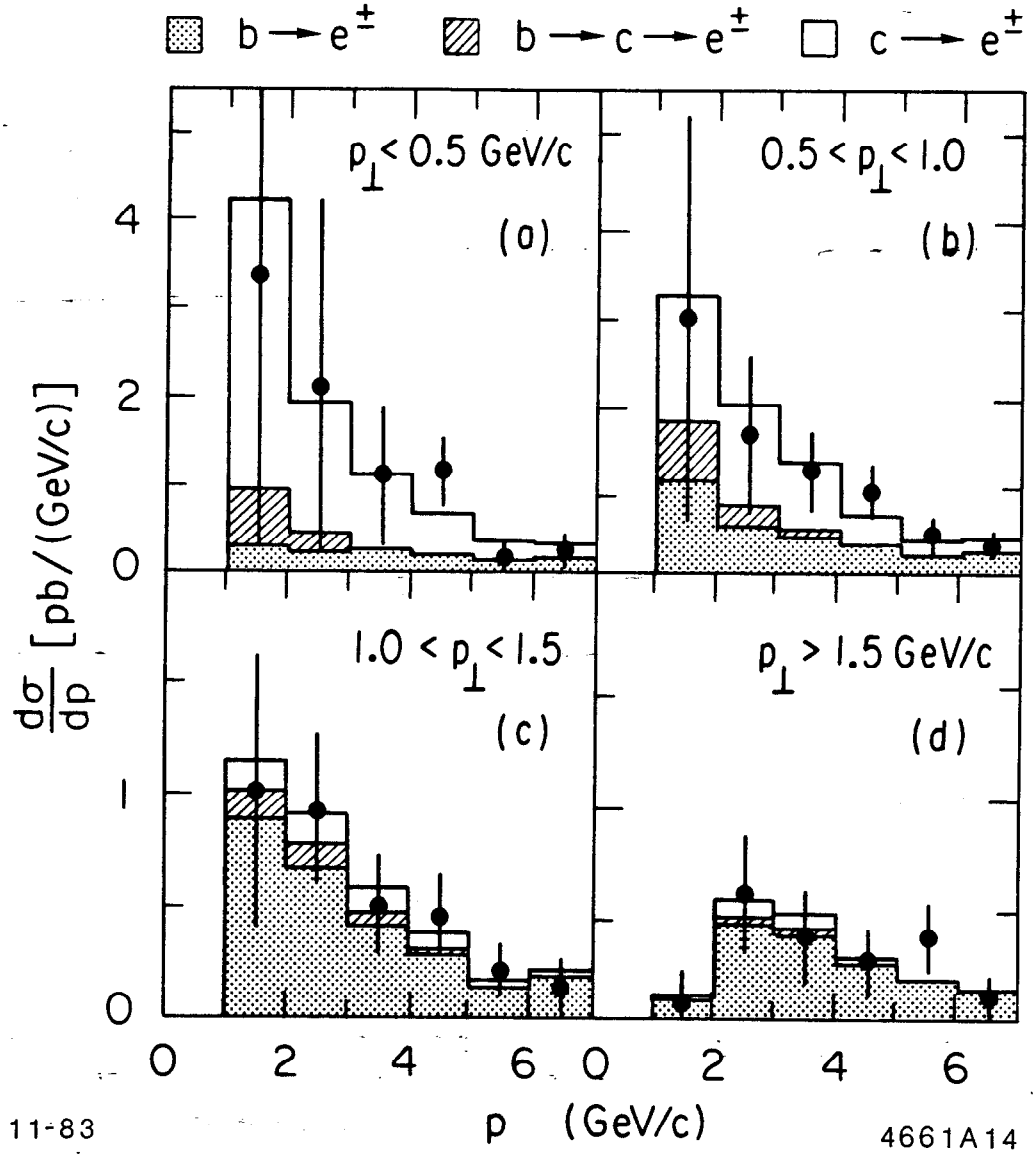

Fig. 4. Prompt-electron momentum spectra in four regions of transverse momentum $p_\perp$ (GeV/c): (a) $p_\perp < 0.5$, (b) $0.5 < p_\perp < 1.0$, (c) $1.0 < p_\perp < 1.5$, and (d) $p_\perp > 1.5$. Two sets of error bars are shown for each data point. The smaller ones are statistical only. The larger ones are the statistical and systematic errors added in quadrature. The highest momentum bin includes all momenta ≥ 6 GeV/c. The histograms show the results of the fit. The three contributions shown are (i) *b* primary (solid), (ii) *c* secondary (diagonally hatched), and (iii) *c* primary (unshaded).

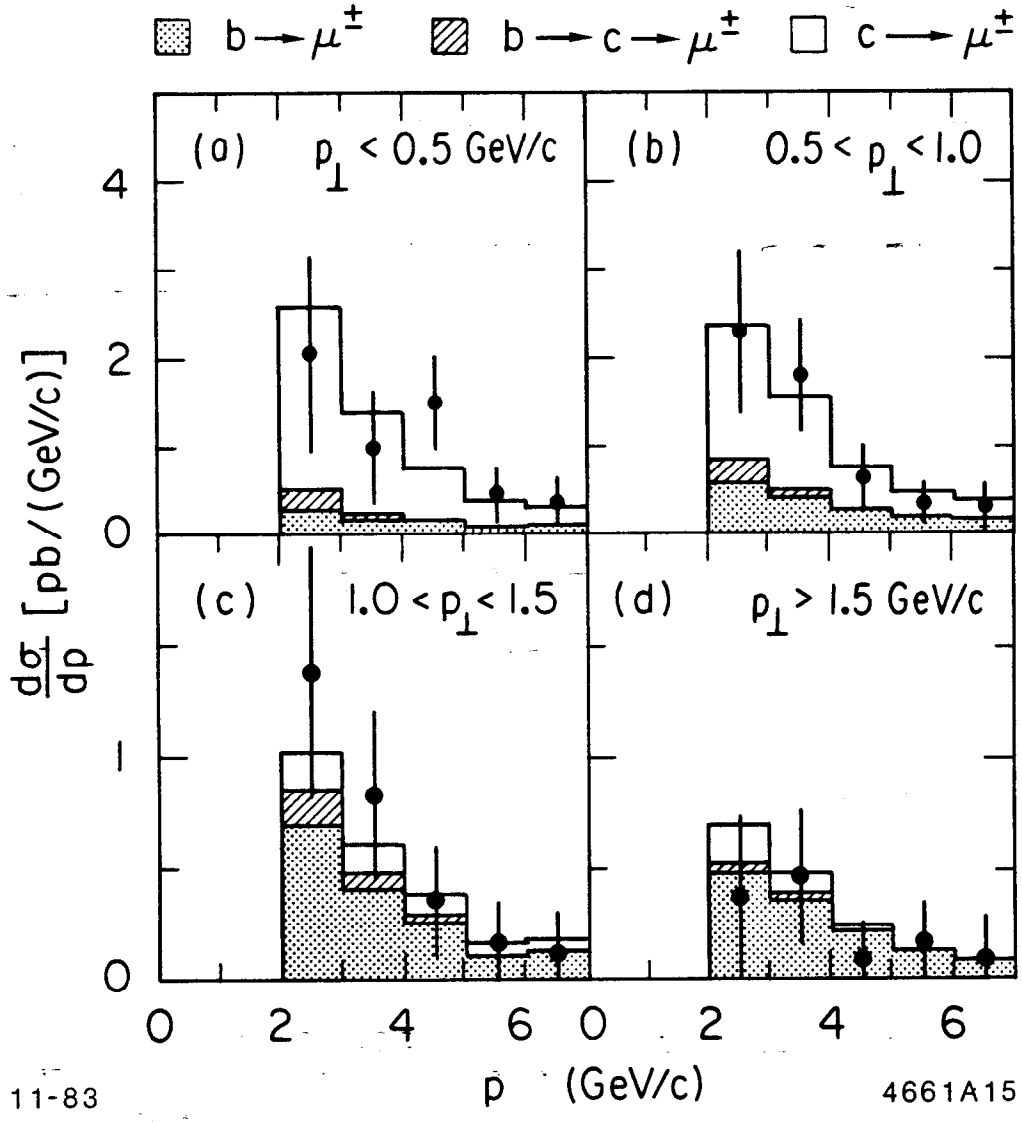

Fig. 5. Prompt-muon momentum spectra in four regions of transverse momentum $p_\perp$ (GeV/c): (a) $p_\perp < 0.5$, (b) $0.5 < p_\perp < 1.0$, (c) $1.0 < p_\perp < 1.5$, and (d) $p_\perp > 1.5$. Two sets of error bars are shown for each data point. The smaller ones are statistical only. The larger ones are the statistical and systematic errors added in quadrature. The highest momentum bin includes all momenta ≥ 6 GeV/c. The histograms show the results of the fit. The three contributions shown are (i) *b* primary (solid), (ii) *c* secondary (diagonally hatched), and (iii) *c* primary (unshaded).

which varies from 78% at 1 GeV/c to 93% at the highest momenta. The misidentification probability varies from 3% at low p and p_T to 0.5% at $p_T > 1.0$ GeV/c. This reflects the difficulty of finding electrons within a tight jet of particles. Conversions and Dalitz pairs are small in number because of the beryllium beam pipe. We remove $\sim 70\%$ of the pairs with a geometrical pair finder.

The background to the prompt muon signal comes from two major sources, pion punch through and π and K decay. There is a few percent probability that a π of $p \sim 2$ GeV/c or more can pass through the four layers of iron absorber without interacting. When combined with the large number of pions per hadronic event this is a significant background to direct muons. The average misidentification probability for punch through is about 0.4%. This varies only slightly with p_T and increases with p, as you expect. We estimate this background using all charged tracks in our hadronic sample. If a given track points at the muon system (we cover 45% of 4π) and has enough momentum to pass through all four layers, it is a candidate track. This track is considered a punch through if it does not reach the fourth layer. We of course take into account range straggling, multiple scattering and electronic inefficiency. We measure the punch through in the first three levels and extrapolate to the fourth level. Therefore we call a muon a charged track which extrapolates into the muon system, and has a hit in each of the four layers within 2σ of the track. Sigma reflects the uncertainty in the track extrapolation from the drift chambers through the calorimeter and the associated multiple Coulomb scattering effects. The effects of π's and K's decaying in flight are determined from Monte Carlo simulation and we find the misidentification probability averages about 0.5%.

Another way of studying these backgrounds is to use samples of pure pions, such as one gets from K°_{S}, τ, and D° decay. Here the statistics are poor, though we have checked they give results consistent with the method described. A more complete description can be found in Ref. 17.

3. Bottom Hadron Lifetime

The b quark lifetime measures the mixing between the second and third quark generations when viewed in the context of the six quark standard model. The preferred decay of the b quark is to its weak isospin doublet partner, the top quark, but this is

obviously not allowed by energy conservation since $m_t > m_b$. The 3×3 quark mixing matrix U_{ij} of Kobayashi and Maskawa (K-M)[18] mixes the weak interaction eigenstates $(d's'b')$ and the mass eigenstates (dsb) using three Cabibbo-like angles θ_i and a phase δ. The unitary K-M matrix can be written

$$U = \begin{pmatrix} U_{ud} & U_{us} & U_{ub} \\ U_{cd} & U_{cs} & U_{cb} \\ U_{td} & U_{ts} & U_{tb} \end{pmatrix} = \begin{pmatrix} c_1 & s_1c_3 & s_1s_3 \\ -s_1c_2 & c_1c_2c_3 - s_2s_3e^{i\delta} & c_1c_2s_3 + s_2c_3e^{i\delta} \\ -s_1s_2 & c_1s_2c_3 + c_2s_3e^{i\delta} & c_1s_2s_3 - c_2c_3e^{i\delta} \end{pmatrix} \tag{2}$$

where $(d's'b') = (dsb)U^T$, U^T is the transposed matrix of U, $c_1 = \cos\theta_1$ and $s_1 = \sin\theta_1$ etc. The U_{ij}'s therefore modify the coupling of the quarks q_iq_j to the intermediate vector boson $W^{\pm}$. The b lifetime can be expressed in terms of simple W emission from the quark line as shown in the spectator diagram for b decay in Fig. 6. The lifetime of the b quark depends on the magnitude of the matrix elements U_{bc} and U_{bu}. We know from the single lepton energy spectrum as measured by CLEO/CUSB[13] at CESR that the $Br(b \to u)/Br(b \to c) < 5.5\%$. This implies the b lifetime predominately measures the matrix element U_{bc}. This has implications to the top quark mass and CP violation.[19,20]

We study the bottom and charm lifetimes by measuring the projected impact parameter of prompt leptons produced in their decays.[21] Bottom is separated from charm kinematically, since leptons with large p_T come principally from the heavier bottom quark. A measurement of the impact parameter distribution for each group, and the knowledge of the relative ratios of bottom and charm populations in each group enable us to disentangle the lifetimes.

The selection of hadronic events is simple and independent of the lifetime of the primary quarks. We search for lepton candidates in those events where the charged energy exceeds .25 $E_{c.m.}$, the center-of-mass energy of 29 GeV. Each event has at least five charged particles, each of which passes within 5 mm of the collision point in the plane perpendicular to the beams and within 7 cm of the collision point along the beam direction. The leptons are identified as described in the previous section.

We ensure the lepton candidate trajectory is well measured in several ways. Each track has a minimum of 13 out of a possible 27 hits in the drift chambers. This is a sufficient number of hits in the drift chambers to allow left-right ambiguities to be

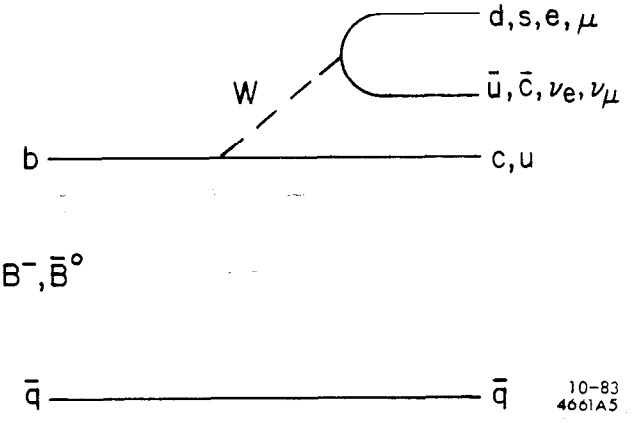

Fig. 6. Spectator diagram for bottom decay.

determined correctly. Using hits from both the inner and outer band of cells in the vertex chamber optimizes the projected resolution after extrapolation to the origin. This is a level arm effect and is described by the equation

$$\sigma^2 = \frac{(r_1^2\sigma_2^2 + r_2^2\sigma_1^2)}{(r_2 - r_1)^2} \tag{3}$$

where the track has transverse errors σ_1 and σ_2 at radii r_1 and r_2. This does not include multiple scattering (see introduction). Each track has at least two hits in the inner band and one hit in the outer band. Furthermore we ensure a good track fit in both the vertex detector and main drift chamber by requiring the χ^2/dof of the track fit to be less than 4.

The direction of the charm or bottom hadron is approximated by the thrust direction. The thrust direction is determined using all charged tracks, including the lepton, which pass loose track quality cuts. The thrust axis for each event has a $|\cos\theta| < 0.7$, measured with respect to the beam direction. This helps contain events within the detector fiducial volume and therefore aids in the accuracy with which we determine the b quark direction.

Leptons with $p_T > 1$ GeV/c and $p > 2$ GeV/c comprise the bottom-enriched sample; those with $p_T < 1$ GeV/c and $p > 3$ GeV/c are the charm sample. The slightly higher cutoff for charm helps reduce the background from the low p, p_T region where the misidentification probability is high. In the b region, $20 \pm 7\%$ of the lepton candidates are nonprompt, which we call background sources; in the c region $34 \pm 9\%$ of the lepton candidates are classified as background. After accounting for background, $80 \pm 8\%$ of the prompt leptons in the b region are from bottom decays and $20 \pm 8\%$ are from charm decays. In the c region, $32 \pm 8\%$ of the prompt leptons are from bottom decays and $68 \pm 8\%$ are from charm decays. The errors quoted are systematic.[17] The errors reflect uncertainties in the lepton decay spectra, the fragmentation functions and the ratio $Br(b \to \ell x)/Br(c \to \ell x)$. The b region is rich in the ratio of bottom decays relative to charm, about 4 to 1, while the c region is only 2 to 1 in the ratio of charm to bottom decays. The b region is less contaminated with background than the c region principally because the electron backgrounds are smaller at high p_T.

The impact parameter δ is the distance of closest approach between the lepton trajectory and the e^+e^- collision point, projected in the plane perpendicular to the

beams. We identify the primary vertex with the average beam position. A positive sign is given to δ if the intersection of the lepton trajectory with the parent hadron trajectory corresponds to a positive decay length, and we assign it a negative δ otherwise. We assume the bottom or charm parent hadron travels from the primary vertex along the thrust direction and decays into a forward going lepton. Negative δ's may arise from mismeasured beam positions or from a parent hadron which decays into a backward going lepton.

The beam position is determined run-by-run by finding the position which minimizes the distance of closest approach for tracks coming from Bhabha and hadronic events. In a typical two hour storage ring fill, we measure the average beam position to within 20μ vertically and 50μ horizontally. The rms beam size is $65 \pm 15\mu$ vertically and $480 \pm 10\mu$ horizontally. The beam position is usually stable during a fill, but in cases of steering, beam position monitors allow us to ignore these runs. In Fig. 7 we show the distance of closest approach divided by the error for both horizontal and vertical tracks from Bhabhas separately. It is a fit to this distribution that yielded the above beam sizes as well as demonstrating that the errors on the measurement are Gaussian and understood, since the widths are very close to unity, with little in the tails. The error on the impact parameter for leptons is dominated by the beam size and ranges from 120μ to 490μ depending on the azimuthal angle of the lepton. The impact parameter error distribution for the leptons is shown in Fig. 8. The shape of the distribution reflects the shape of the beam, small in the vertical and large in the horizontal. We accept only those lepton candidates with $\sigma_\delta < 350\mu$, which leaves 307 leptons for the remaining analysis.

The measured lepton impact parameter distributions are shown in Fig. 9(a) for the b region and Fig. 9(b) for the c region. Only tracks with $|\delta| < 1$ mm are considered when computing the averages and in making the fits to the data. We do this to help reduce the effects of the tails on the final answer. The mean of the b enriched plot is $106 \pm 29\mu$ and of the c enriched plot is $63 \pm 18\mu$. The dominant background for electrons and muons is misidentified hadrons. We have measured the impact parameter distribution for nonleptons in the b region and c region, weighting the sample in p, p_T space according to the misidentification probability. Only one hadron track per event enters the histogram and this track passes all quality cuts normally applied to the

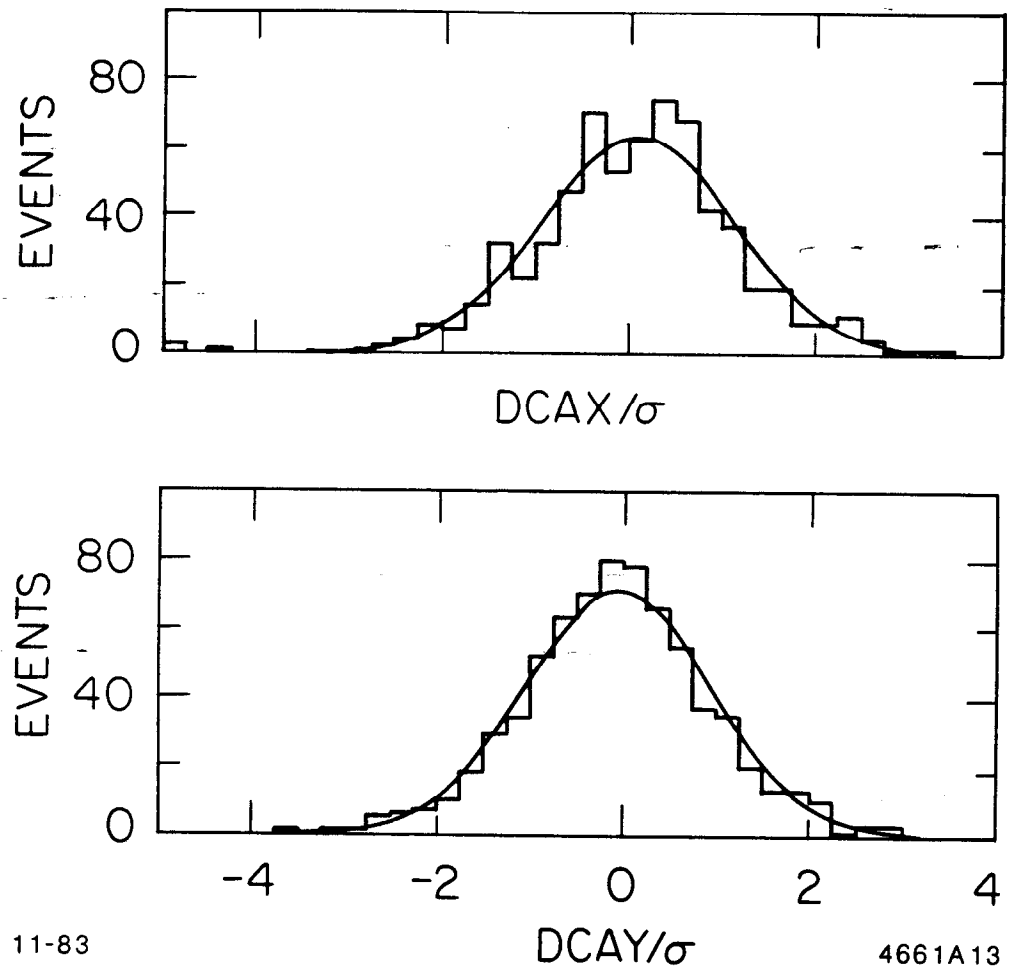

Fig. 7. The top graph is the distance of closest approach of horizontal Bhabha tracks DCAX with respect to the beam position divided by the individual errors on each measurement. A fit to a Gaussian yields a vertical beam size of 65 μm. The lower graph uses vertical Bhabhas and the fit yields a horizontal beam size of 480 μm.

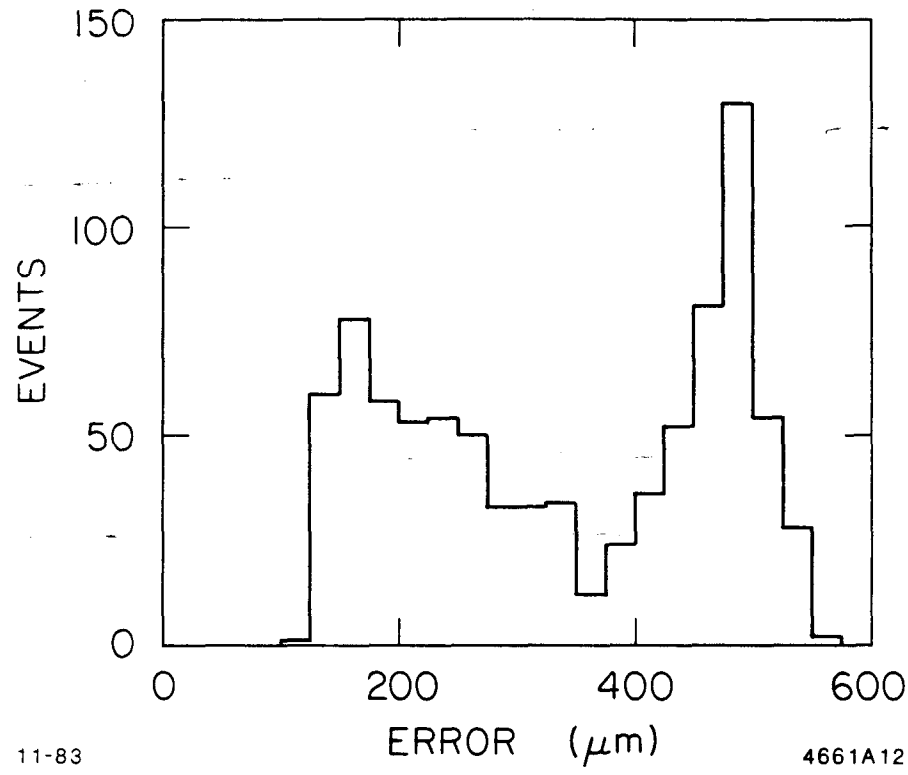

Fig. 8. Distribution of impact parameter errors for leptons in the bottom enriched and charm enriched regions. Events with an error $\leq$ 350 micron are accepted.

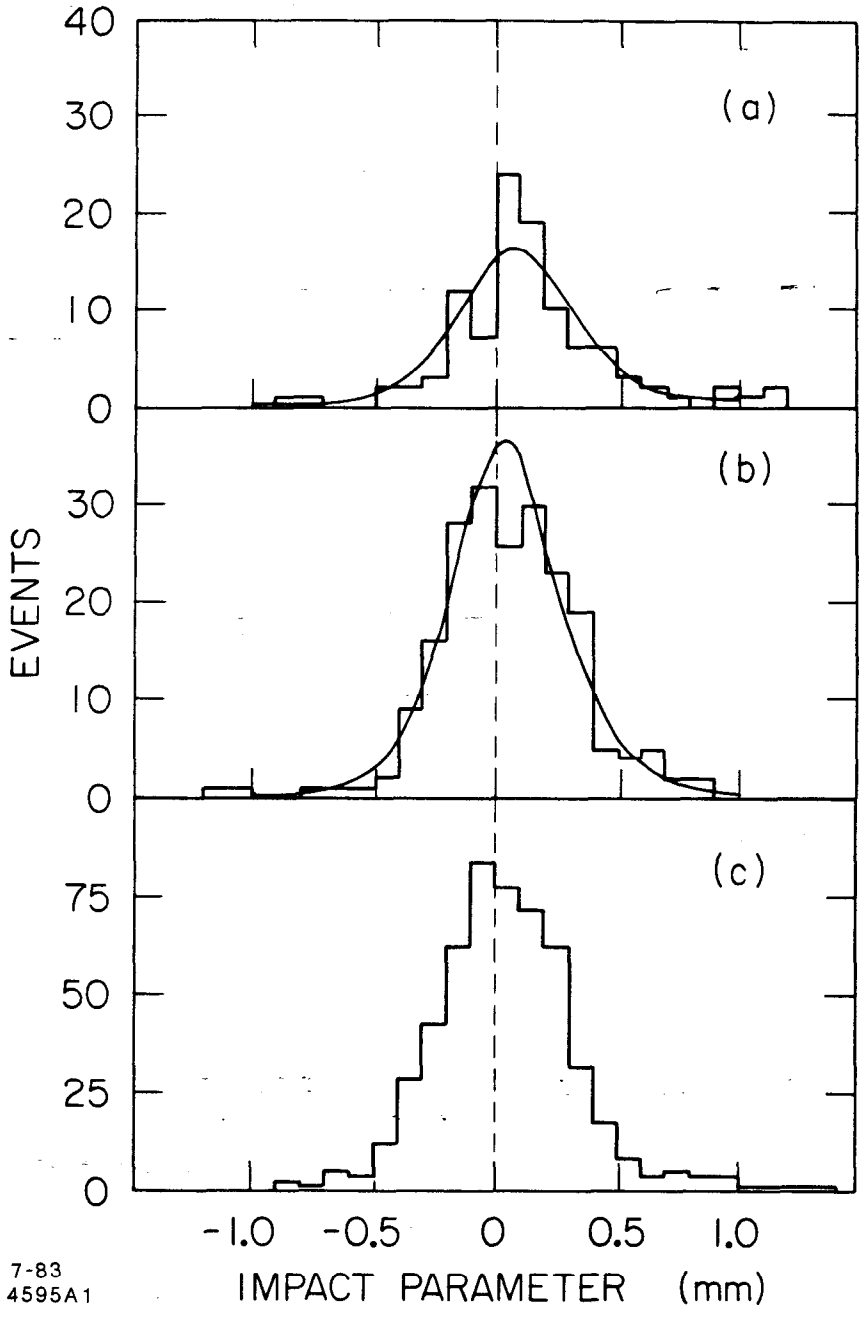

Fig. 9. Impact parameter distributions for (a) leptons in the b region; (b) leptons in the c region; (c) hadrons in the b region. The solid curves are the result of the fit described in the text.

leptons. The background from conversions are negligible because very little material (0.6% of a radiation length) preceeds the tracking chambers. Conversions after the inner band of the cells in the vertex chamber are eliminated by the minimum hit requirement in this band and remaining conversions are removed with a 70% efficient geometrical pair finder. The impact parameter distribution for the pion and kaon decay background is similar to that for nonleptons. Further, since the thrust axis does not in general follow the direction of the decaying pion or kaon, the sign of the impact parameter may be positive or negative thereby reducing the concern that this background leads to a positive definite impact parameter distribution. The impact parameter distribution for the hadrons in the b region is shown in Fig. 9(c) and for hadrons in the c region in Fig. 10. The average impact parameter of hadrons in the b region is $36 \pm 12\mu$ and in the c region it is $12 \pm 7\mu$.

Lifetimes are extracted from the two lepton impact parameter distributions, b region and c region, by fitting simultaneously for a bottom and charm lifetime using a maximum likelihood technique, after accounting for the background. We consider the impact parameter distribution in the b or c (i = 1,2) region to be composed of three distributions; a normalized shape for the background $dn/d\delta_{hi}$ weighted by the fraction of background f_{hi}, and a shape for the bottom and charm decay's impact parameters weighted in proportion to their respective populations, $(1 - f_{hi})f_{bi}$ for b's and $(1 - f_{hi})(1 - f_{bi})$ for c's. The normalized impact parameter distributions $dn/d\delta_i$ can then be written

$$\frac{dn}{d\delta_i} = f_{hi}\,\frac{dn}{d\delta_{hi}} + (1 - f_{hi})\left[f_{bi}\,\frac{dn}{d\delta_{bi}} + (1 - f_{bi})\,\frac{dn}{d\delta_{ci}}\right] \quad . \tag{4}$$

The normalized impact parameter distributions $dn/d\delta_{bi}$ for b decay and $dn/d\delta_{ci}$ for c decay are computed by convoluting the 'true' impact parameter distribution with our experimental resolution, a Gaussian centered on zero of width σ_δ, on an event by event basis. We calculate the 'true' impact parameter for b and c decay in both the b and c regions using Monte Carlo techniques which include the experimental lepton spectra[13] and kinematic selection criteria but no detector resolution effects. There are four such distributions, one of which is shown in Fig. 11, the other three are similar. They are peaked at low impact parameter, have exponentially decreasing tails, and scale with the lifetime of the parent hadron. Roughly 6% of the bottom decays are

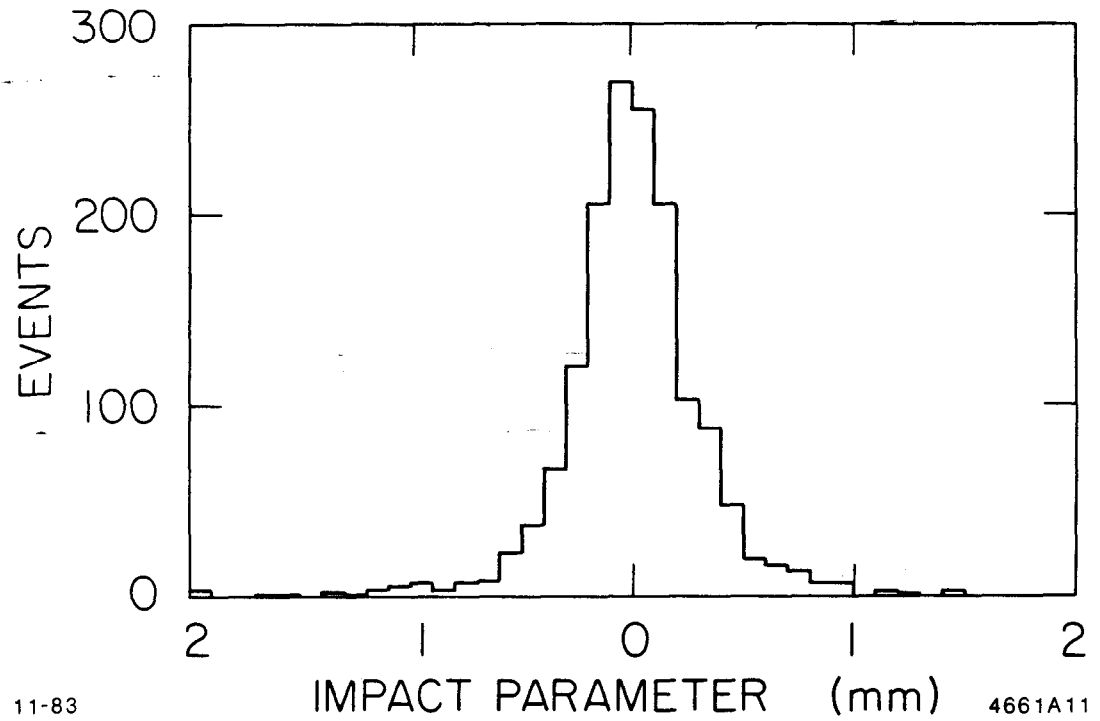

Fig. 10. Impact parameter distributions for hadrons in the c region.

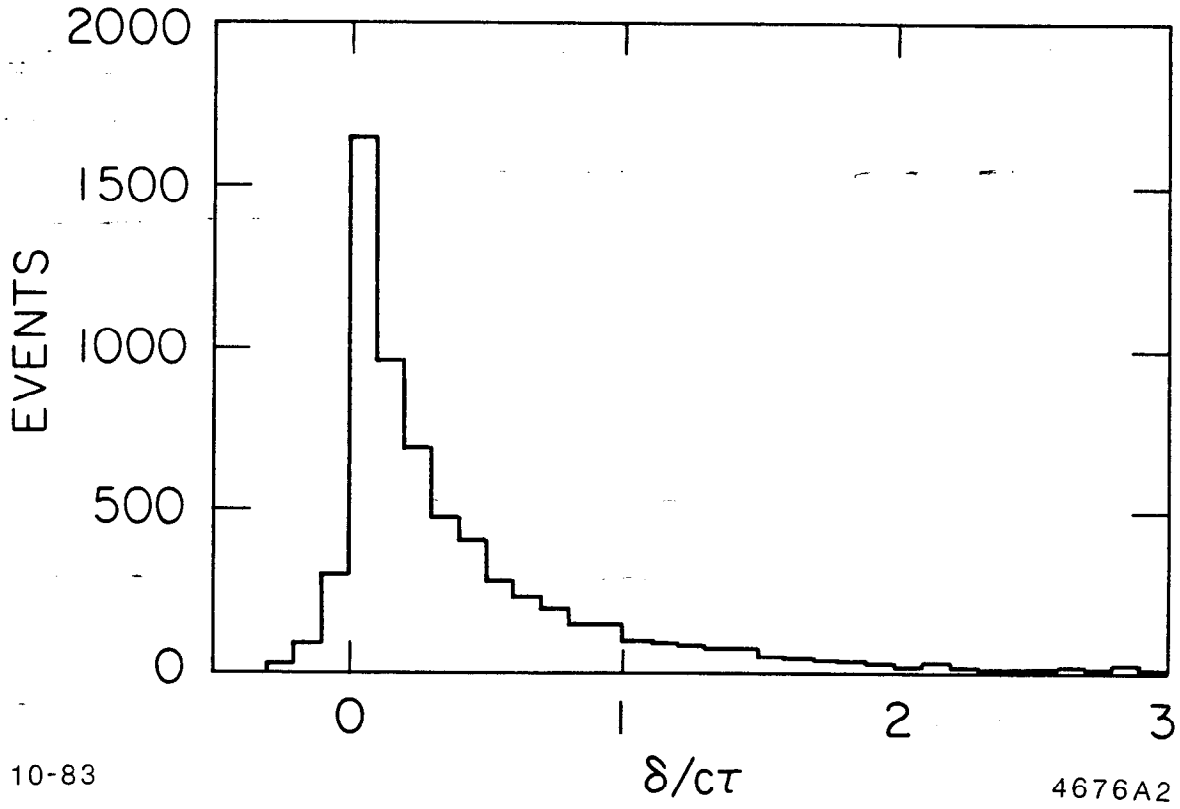

Fig. 11. Monte Carlo produeed distribution of impact parameters divided by $c\tau$ for leptons produced in bottom decays. The above represents events in the b region.

backwards and this is accounted for by the small negative impact parameters in the b distributions. The average impact parameter from b decays is about $135\mu/10^{-12}$ sec in the b region and $70\mu/10^{-12}$ sec in the c region; for charm decays it is about $120\mu/10^{-12}$ sec in the b region and $95\mu/10^{-12}$ sec in the c region. The b region with its high $\langle p_T \rangle$, preferentially selects large angles with respect to the thrust axis and therefore larger impact parameters than does the low $\langle p_T \rangle$ of the charm sample.

The result of the fit is summarized in Fig. 12 which shows equal likelihood contours in the $\tau_c - \tau_b$ plane. The plot shows substantial correlation between the two lifetimes. From our own data we find $\tau_b = \left(10.3^{+\ 5.2}_{-\ 4.2}\right) \times 10^{-13}$ sec and $\tau_c = \left(8.3^{+\ 5.1}_{-\ 4.8}\right) \times 10^{-13}$ sec. We can obtain a more precise value of τ_b by using world data on charm lifetimes. We estimate the appropriate average to be $\tau_c = (6.0 \pm 1.5) \times 10^{-13}$ sec, where we have taken into account the large D^* production at PEP, and the measured lifetimes and branching ratios of the charmed particles. The quoted error includes the uncertainties in both individual lifetimes and relative production rates of the various charmed particles. After refitting with this estimate, which agrees within errors with our own τ_c measurement, we find $\tau_b = \left(12.0^{+\ 4.5}_{-\ 3.6}\right) \times 10^{-13}$ sec.

We have checked that with input lifetimes found above for bottom and charm; a Monte Carlo simulation of the background yields $37 \pm 24\mu$ in the b region and $14 \pm 12\mu$ in the c region, in good agreement with the measured values. Furthermore we determined the bottom hadron lifetime from the electron and muon samples separately, and found they agree within errors. The background distributions themselves offer a good general check that geometric alignment, mistracked tracks, or incorrect beam positions are not the source of the shift observed by the leptons. Since the backgrounds were handled identically to the leptons the only difference in the two samples is the number of tracks which come from bottom hadrons. Simply, high p_T leptons tag bottom hadrons more efficiently than just high p_T hadrons. The measurement technique has been checked with Monte Carlo simulated data, and we found that fitted lifetimes agreed with input lifetimes to within the statistical errors.

The systematic error derives principally from the uncertainties in the background fractions, bottom-hadron fractions, fragmentation functions and fitting procedures. The above lead to a 25% uncertainty in the bottom hadron lifetime.

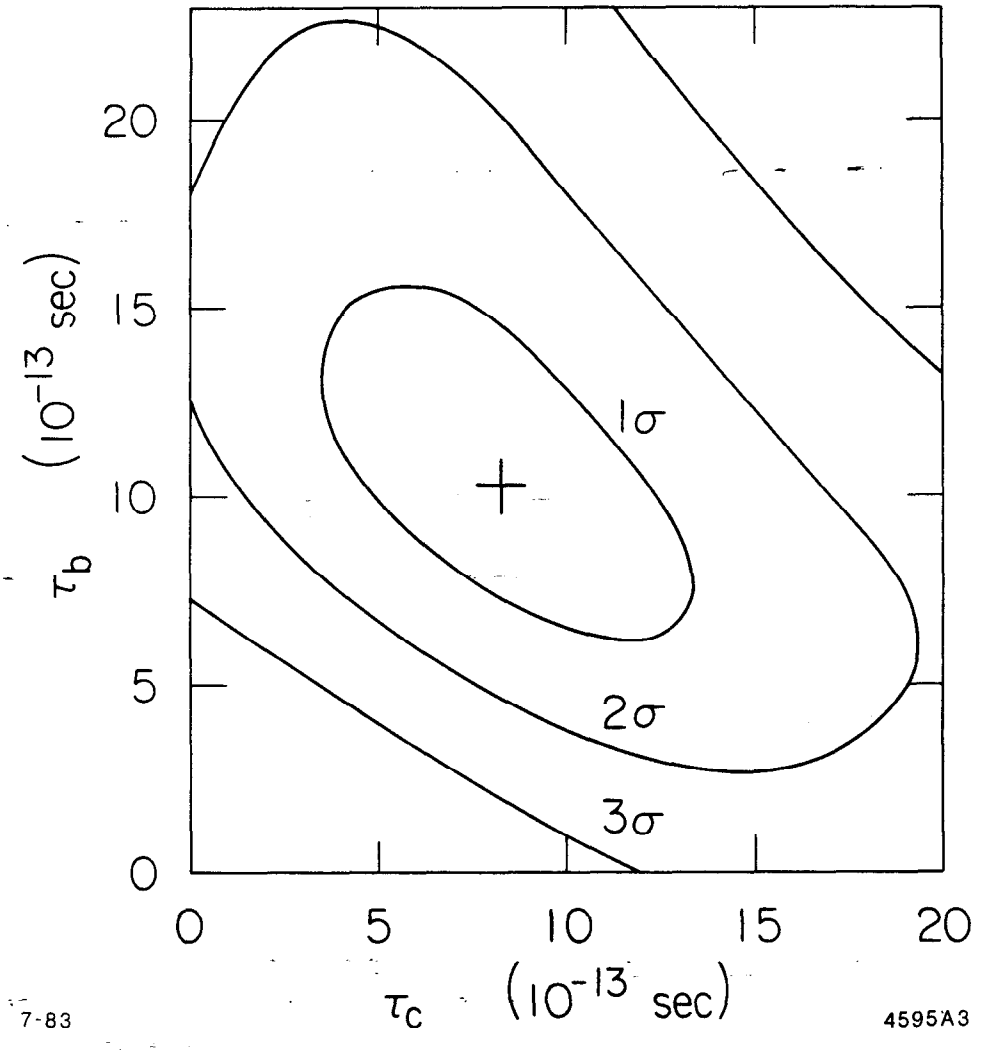

Fig. 12. Equal likelihood contours in the $\tau_c - \tau_b$ plane, corresponding to one, two, and three standard deviations from the best fit values.

In summary, we have measured the average lifetimes of bottom hadrons and found $\tau_b = \left(12.0 \pm {}^{4.5}_{3.6} \pm 3.0\right) \times 10^{-13}$ sec. This lifetime represents an average over bottom hadron species, weighted by the product of their respective production cross sections and semileptonic branching ratios. This measurement of τ_b is consistent with the value presented at this conference by M. Piccolo of the MAC Collaboration.

The bottom hadron lifetime has relevance to the top quark mass and CP violation[19,20] because it significantly constrains the magnitude of the K-M mixing matrix parameters. The bottom hadron lifetime has been related to the K-M matrix elements by Gaillard and Maiani:[22]

$$\tau_b = \frac{\tau_b^\circ}{(2.75|U_{bc}|^2 + 7.7|U_{bu}|^2)} \quad . \tag{5}$$

Here $\tau_b^\circ = \tau_\mu (m_\mu/m_b)^5$, where τ_μ is the muon lifetime and m_μ/m_b is the ratio of the muon and b quark masses. As stated earlier, the limit on the ratio $Br(b \to u)/Br(b \to c) < 5.5\%$ [13] implies that $|U_{bu}|^2 < 0.02|U_{bc}|^2$, so we consider U_{bu} negligible in Eq. (5). Using $m_b = 5$ GeV/c^2 we find $|U_{bc}| = 0.053 \pm {}^{.010}_{.009}$, statistical errors only. This can be compared to the sine of the Cabibbo angle, $U_{su} = 0.22$, about four times larger.

The calculation of the CP violating amplitudes in the $K^\circ - \bar{K}^\circ$ system involve products of the K-M angles $\sin\theta_2 \cos\theta_2 \sin\theta_3 \sin\delta$ or $s_2 c_2 s_3 s_\delta$. Using the above information, the b lifetime and the $Br(b \to u)/Br(b \to c)$, one can place a lower bound on $s_2 c_2 s_3 s_\delta$ and therefore ϵ'/ϵ.[23,24] Here ϵ' is a measure of direct CP violation in the decay $K_L \to 2\pi$, and ϵ is the dominant contribution which arises from the CP impurity of the K_L. A different approach uses the experimental value of ϵ as a constraint and proceeds to calculate a lower bound on the top quark mass as a function of the b lifetime.[20] All of this hinges on the existence of the top quark and, at present, considerable theoretical uncertainties.

Finally, it is clear that a statistically more significant b lifetime measurement is needed. We hope to obtain greater precision in the lifetime by reducing the uncertainty in the position of the primary vertex by using tracks within the event. In addition, we are attempting to measure the lifetime by a path length technique.

4. Precise Measurement of the Tau Lifetime

The tau lepton is expected to couple to the charged weak current with the universal Fermi strength in the standard model. This universality assumption for the third lepton generation is tested by a measurement of the tau lifetime. Since the lifetime can be calculated to better than 10% within the context of the standard model,[25] a measurement of equivalent precision is desirable.[26–28] We present here a new measurement of the tau lifetime based on an integrated luminosity of 41 pb^{-1} which has been made using our high precision vertex detector.[3]

The tau lifetime is determined by measuring the distribution of displacements between the e^+e^- collision point, which we identify with the beam position, and the vertex of the three prong decay mode of the tau. We can calculate the lifetime from this distribution since the tau is produced with the beam energy and thus the relativistic gamma factor is known.

The selection of $1+3$ and $3+3$ event topologies of the tau can be made with very little background at the PEP $E_{c.m.}$ of 29 GeV. The tau direction is assumed to lie along the direction of the 3 prong system. The average beam position is determined run-by-run, using the same method as described earlier for the bottom hadron lifetime analysis. The projected decay length is given by

$$\ell_p = \frac{x_v\sigma_{yy}t_x + y_v\sigma_{xx}t_y - \sigma_{xy}(x_vt_y + y_vt_x)}{\sigma_{yy}t_x^2 + \sigma_{xx}t_y^2 - 2\sigma_{xy}t_xt_y} \tag{6}$$

where (x_v, y_v) is the decay vertex position relative to the beam position, σ_{ij} is the sum of the beam and vertex error matrices, and t_i are the projected τ direction cosines. The decay length is then $\ell = \ell_p/\sin\theta$, where θ is the angle between the tau and beam directions. Figure 13 shows the decay length distribution for 156 decays where the resolution on each decay length has been required to be less than 1700μ. The resolution on the decay length depends on the 3 prong opening angles, track momenta, and orientation of each decay and varies between 500μ and 1800μ for most decays and averages $\sim$ 1100μ.

We use a maximum likelihood fitting procedure to extract the lifetime from the decay length distribution. The fitting function is a convolution of an exponential decay length distribution and a Gaussian resolution function of width σ_ℓ, calculated event by event. The Gaussian is centered on zero. The result of the fit, which yields a mean

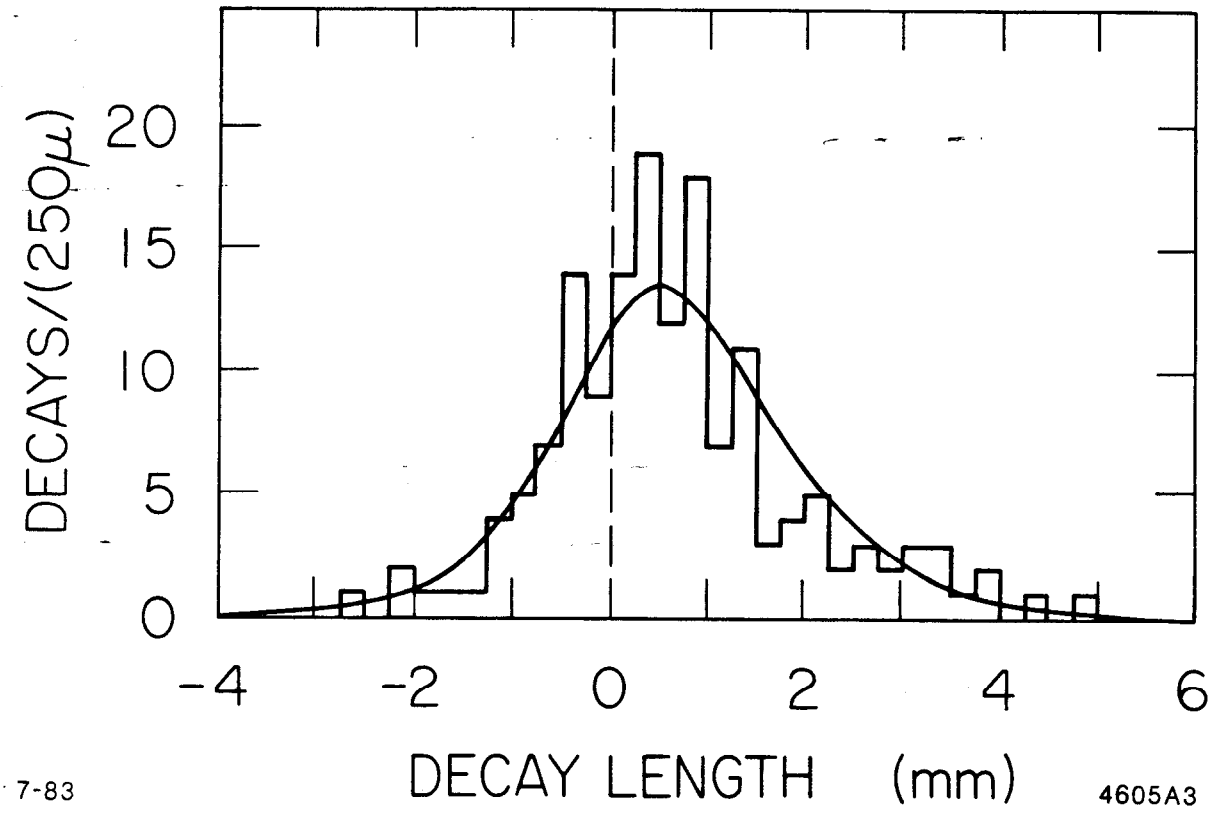

Fig. 13. Measured τ decay lengths. The solid curve is the best fit to the data.

decay length of $705 \pm 87\mu$ (statistical), is shown superimposed on the data in Fig. 13, and describes the data well. We find $\tau_\tau = (3.20 \pm 0.41) \times 10^{-13}$ sec after correcting for the small amount of background ($+30\mu$) and the effects of initial state radiation. This is to be compared with the expected value $\tau_\tau = \tau_\mu (m_\mu / m_\tau)^5 B_e = 2.8 \pm 0.2 \times 10^{-13}$ sec where $\tau_\mu(m_\mu)$ is the muon lifetime (mass) and B_e is the tau branching ratio into $e\nu\bar{\nu}$.[29]

A sample of tracks which simulate the momentum and topology of tau decays was constructed in order to check for bias in the fitting technique and measurement. We selected a sample of 3 prongs from hadronic events and excluded tracks coming from K_S^0 decay and the highest momentum track in a jet to suppress tracks not coming from the e^+e^- collision point. The decay length distribution for this control sample is shown in Fig. 14(a). The fitted mean decay length is $72 \pm 38\mu$. From Monte Carlo studies we find this procedure gives decay lengths in the range 50μ to 150μ depending on the D^+/D° ratio and the bottom lifetime. The width of the resolution function is important in our fitting procedure. In Fig. 14(b) we show the decay length divided by its error for the control sample. A unit-width Gaussian describes the data well and we determined the width of the resolution function is correct to 5%.

We have studied several sources of systematic error. One measurement bias comes from mismeasurement of the track angles, or simple multiple scattering of the tracks from tau decay. Tracks that scatter or are mismeasured to larger angles extrapolate back to give longer decay displacements from the collision point. Larger opening angles gives smaller vertex errors and hence these longer lived events carry proportionately more weight in the fit. In previous determinations of the tau decay length,[26–28] corrections of $\sim 250\mu$ were made to compensate for this effect. This measurement has reduced this effect to $\sim 25\mu$ by having reduced multiple scattering and improved track resolution. The uncertainties in the resolution function, background corrections, and other uncertainties in the analysis lead to a systematic error of 80μ.

In summary, we have measured the tau lifetime to be $\tau_\tau = (3.20 \pm 0.41 \pm 0.35) \times 10^{-13}$ sec, where the first error is statistical and the second is systematic. This analysis was based on 41 pb^{-1} and further improvements in the lifetime must await a better understanding of the systematic errors involved. We will certainly continue this work in order to provide an even better test of $e - \mu - \tau$ universality.

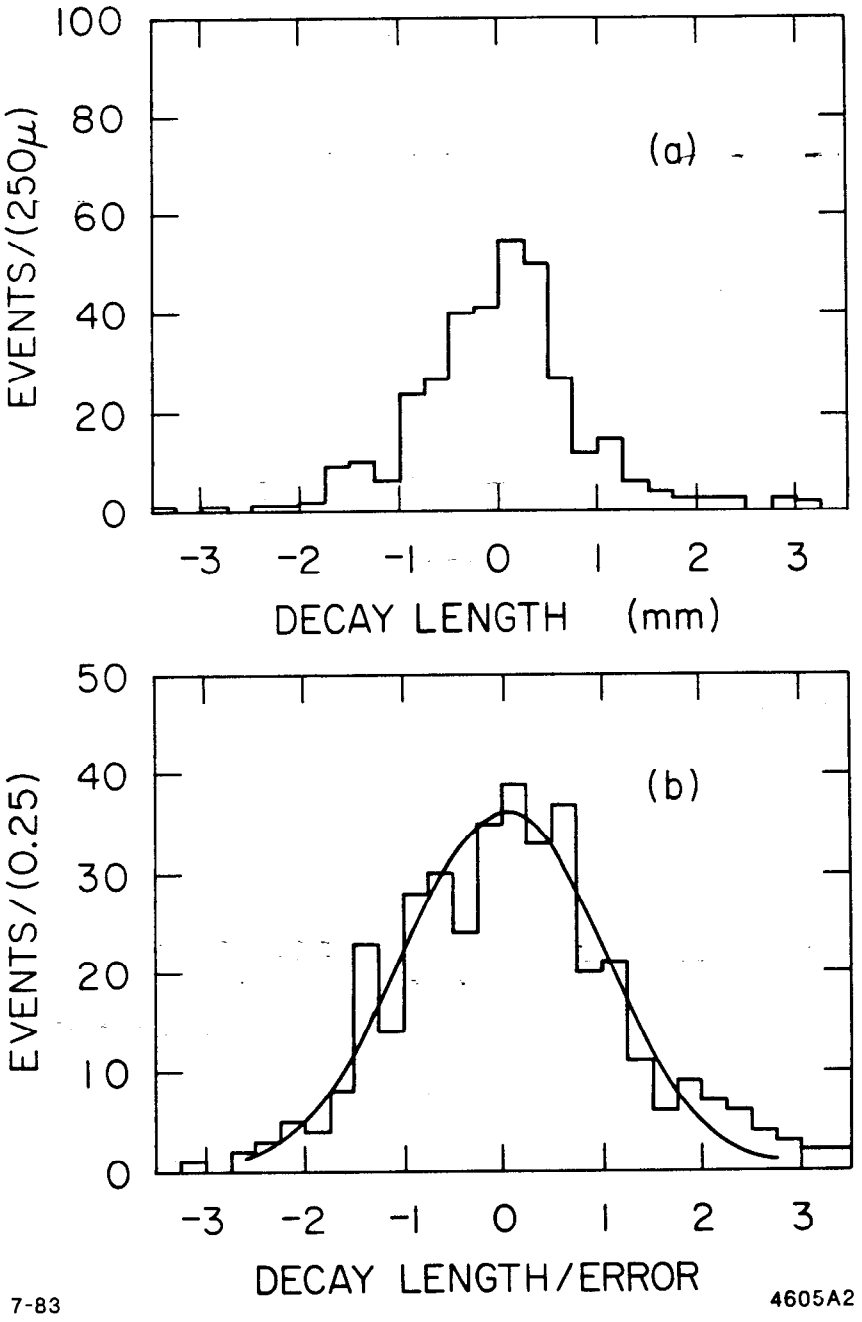

Fig. 14. (a) Measured decay lengths for "pseudo-τ" decays; (b) decay length divided by its calculated error for pseudo-τ decays. The solid curve is a unit-width Gaussian function, normalized to the data between $-2.5 \leq \ell/\sigma \leq 2.5$.

5. D° Lifetime

The measurement of charm lifetimes has been an area of considerable experimental activity over the last few years. Of particular interest is the ratio of $\tau_{D^+}/\tau_{D^\circ}$, which gives information about the relative strengths of the spectator and nonspectator amplitudes. Since there is no nonspectator diagram for the D^+, it is expected to have a longer lifetime than the other charm particles (if nonspectator diagrams are important). The MARK II at present can contribute information on the lifetime of the D° meson only. Here we report preliminary results based on a small clean sample of D°'s. The detection method and analysis procedure used to identify the D° meson is independent of the D° lifetime.

The sample of D° mesons used is obtained by observing the decay

$$\begin{aligned} D^{*+} &\to D^\circ \pi^+ \\ &\to K^- \pi^+ \quad . \end{aligned}$$

It has been shown previously[30] that this decay can be isolated with very little background at high values of z, where z is twice the energy of the D^{*+} divided by $E_{c.m.}$. For this analysis, all particles were tried as pions or kaons, and all oppositely charged kaon pion pairs with invariant mass of $1.72\ \mathrm{GeV/c^2} < M_{K\pi} < 2.00\ \mathrm{GeV/c^2}$ were taken as D° candidates. With their momenta constrained to the D° mass, each D° candidate was then combined with the additional pions in the event and those combinations with a small mass difference $(M_{D\pi} - M_D)$ were called D^{*+} candidates. Further cuts were then applied to ensure that the production point of the D° was well measured by the vertex chamber. In addition, a well constructed D° decay vertex was ensured by accepting only those decay vertices with a $\chi^2/\mathrm{dof} < 5$. This cut discriminates against events where tracks from the D° have scattered or been mismeasured. The mass difference after all cuts is shown in Fig. 15. D^{*+} events were defined to be those with a $z_{D^*} > 0.6$ and a mass difference of $143 < (M_{D\pi} - M_D) < 149\ \mathrm{MeV/c^2}$. A total of 20 well measured events are seen in the D^{*+} region, and no other combinations are shown. We estimate a background of about $1\frac{1}{2}$ events. It is estimated that at most 5% of the D^{*+}'s with $z > 0.6$ originate from bottom meson decays.

The decay length for each observed D° decay was calculated as the distance between the D° vertex and the e^+e^- collision point, taken to be the average beam position

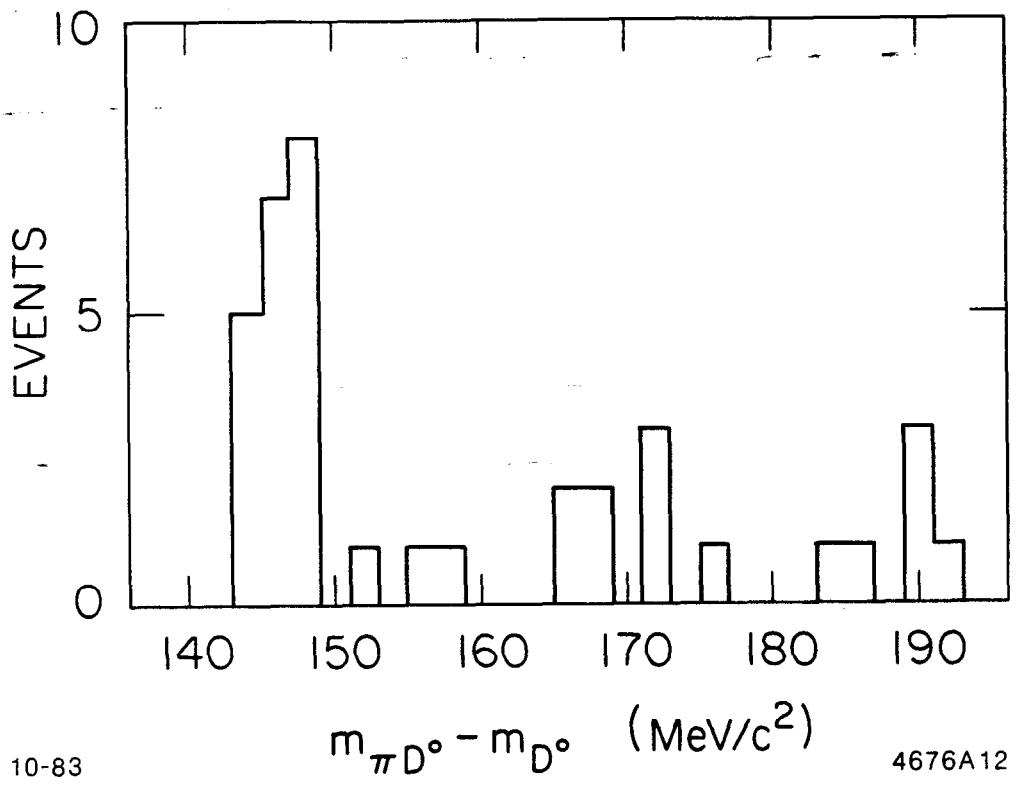

Fig. 15. The mass difference $(m_{\pi D^0} - m_{D^0})$ for D^{*+} candidates with $z > 0.6$ (preliminary data).

for a run. The measurement took place in the plane perpendicular to the beam direction and then corrected for the polar angle using the D^0 direction. The properties of the beam and the fitting procedure have been described in the sections on the tau lifetime and b lifetime. The 20 individual measurements of the lifetime shown in Fig. 16. The most probable mean decay time for the D^0 was found using a maximum likelihood fit to an exponential decay distribution, convoluted with Gaussian errors, the individual errors being retained. The result of the fit gives $\tau_{D^0} = \left(4.0 \pm {}^{1.4}_{1.1}\right) \times 10^{-13}$ sec, where the error is statistical.

To check for biases in the vertexing and fitting procedure we used Monte Carlo simulated data for D^0 production and decay. For several mean input lifetimes, the analysis method yielded these lifetimes within the statistical errors. As a further check, we constructed a sample of "pseudo D^0's" from tracks in hadronic events having similar topology and kinematics to that of the D^0 events. Tracks giving an invariant mass consistent with a K^0_S were removed. The mean lifetime of the fake D^0's was found to be slightly positive. This was expected since some candidate tracks came from heavy quark decays. From the above and other considerations we estimate the systematic error to be 1.0×10^{-13} sec.

In summary, we have measured the D^0 lifetime to be $\tau_{D^0} = \left(4.0 \pm {}^{1.4}_{1.1} \pm 1.0\right) \times 10^{-13}$ sec where the first error is statistical, the second systematic. The analysis was based on ~ 100 pb^{-1} yielding 20 well measured events with small background. This measurement is consistent with all other measurements of the D^0 lifetime using different techniques.

6. A Search for Supersymmetric Electrons

Supersymmetric theories[31] associate fermions and bosons in multiplets such that all known particles have supersymmetric partners whose spins differ from ordinary particles by $\pm 1/2$. Each supersymmetric particle has the same electromagnetic and weak couplings as its partner, although its mass may be different because of symmetry breaking. It is possible that all superpartners have large masses compared to M_W, in which case evidence supporting the theory will have to wait for some time. Supersymmetry has been popular since it helps solve the hierarchy problem of the standard gauge theories.[32] At present, there is no experimental evidence supporting the existence of any superpartners.

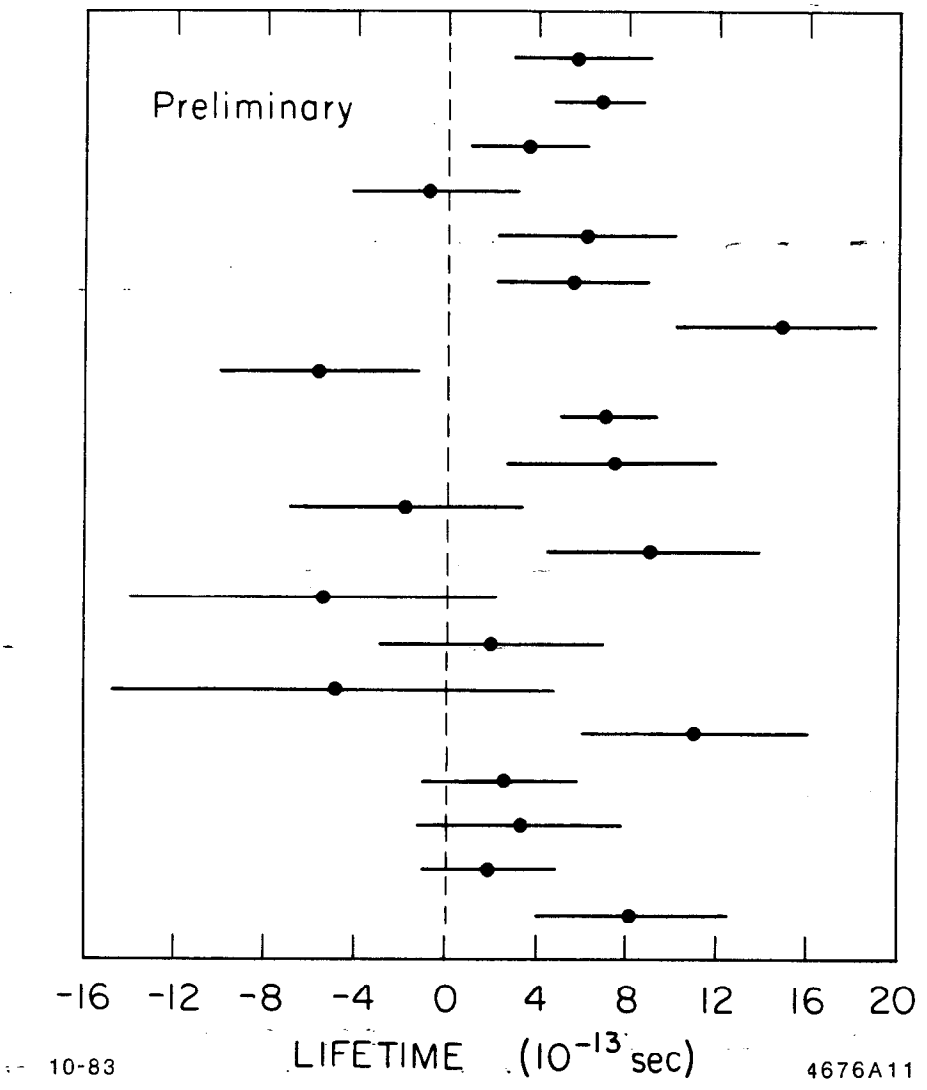

Fig. 16. The individual measurements of the lifetime for the 20 D^o candidates.

We have made a search for the selectron, $\tilde{e}$, the supersymmetric partner of the electron. It can be singly produced in association with photinos, $\tilde{\gamma}$ (spin -1/2, neutral partner of the photon), through the reaction $e^+e^- \rightarrow e^{\pm} + \tilde{e}^{\mp} + \tilde{\gamma}$. The Feynman graphs for this production are shown in Fig. 17. The produced selectron is assumed to decay rapidly into a photino and electron. The photinos are assumed to be massless and noninteracting. This gives a distinct experimental signature; one hard electron detected with large transverse momentum relative to the beam axis.[33] This procedure allows us to extend the mass range of the search to 75% of the $E_{c.m.}$. This is of course in contrast to previous pair production searches which are limited to masses no greater than 50% of the $E_{c.m.}$.[34–36]

Several properties of the detector not mentioned earlier are important for this search. Charged particles can be detected to within 10° of the beam axis using the inner band of wires in the vertex detector. The small angle tagging (SAT) system consists of four semicircular modules, with two on either side of the main detector. This calorimeter covers the forward and backward cones between 2° and 4° from the beam axis, and is 15 radiation lengths (X_0) thick. The endcaps have an acceptance of $0.75 < |\cos\theta| < 0.92$, and are approximately $5X_0$ thick but have a substantial break in their azimuthal coverage due to their support stand.

The following criteria were applied to all events which passed the trigger requirement; one charged track depositing at least 1 GeV in the LA calorimeter. First, in order to measure the energy of the charged track reliably, we required the particle to have $|\cos\theta| < 0.70$ and to miss the azimuthal gaps between the modules by at least 2.7°. The detected track was called an electron if it deposited at least 6 GeV in the LA module. This also helped eliminate background from two-photon production of low energy electrons. To eliminate cosmic ray showers, tracks were required to originate from the beam luminous region and the event was required to have less than 50 hits in the drift chambers. Events containing photons were ignored unless they were within 10° of the track, which would be consistent with an electron radiating in the detector material before the LA system. In addition we confined all unseen particles to within 2° of the cone about the beam axis by requiring no evidence for low angle tracks in the vertex detector or energy deposit above 3 GeV in the SAT shower counters. After the above cuts we were left with 763 events to analyse. One further cut was applied to these events after a study of the background sources.

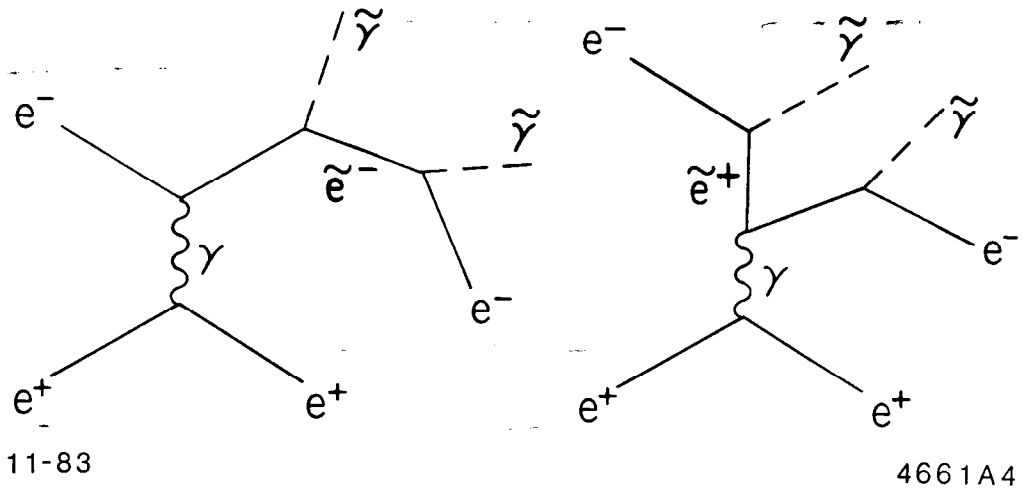

Fig. 17. Diagrams for production of a single supersymmetric electron in e^+e^- annihilation.

The major sources of background in this search are QED processes, in particular $e^+e^- \rightarrow e^+ + e^- + \gamma$ ($ee\gamma$) where one electron is detected, one goes down the beam axis at a small angle and the gamma falls into a dead or inefficient region of the calorimeter. The three body kinematics of these events, together with the confinement of the unseen electron to within 2° of the beam axis allows the gamma direction to be determined. The accuracy of predicting the gamma direction was checked by using events in which the gamma is detected. Figure 18 shows a plot of $\chi_{\cos}$, the normalized error distribution in the cosine of the gamma polar angle, ($\cos\theta_\gamma$), with a Gaussian fit superimposed. The fit, which did not include the tails, fits the data well and supports the three body hypothesis. The tails are assumed to arise from higher order QED processes and non-Gaussian tails in the experimental resolution. The distribution of deviations in the azimuthal angle was found to have a FWHM of 0.02 radians. In addition, we have studied the angular distribution of the detected photons in the $ee\gamma$ events. From this we calculate that 266 events with an undetected photon fall into the dead region of our calorimetric acceptance ($\cos\theta$ between 0.715 and 0.750, between the LA system and the endcap). This number and the resolution determined from Fig. 18 suggest a cut of $|\cos\theta_\gamma| < 0.54$ would reduce the $ee\gamma$ background to less than one event. After this cut the efficiency for high mass selectrons remains $\sim 40\%$ since their angular distribution is quite uniform. The additional backgrounds coming from higher order QED processes such as $ee\gamma\gamma$, tau production and two photon processes were found to be small.

The effect of all cuts used in this analysis defines an acceptance shown in Fig. 19 for a single (negatively) charged prong. The data points shown are consistent with the known background estimates. The search yielded no final candidate events for an integrated luminosity of 123 pb^{-1}. This yields a 95% confidence level upper limit on the cross section within the acceptance of Fig. 19 of 2.4×10^{-2} pb.

Finally, we set an upper limit on the cross section for selectron production as a function of the selectron mass. The cross section of Ref. 33 was integrated over the acceptance and is shown in Fig. 20. The upper limit on the cross section gives a 95% confidence level lower limit on the mass of the selectron of

$$M_{\tilde{e}} > 22.2 \text{ GeV/c}^2 \quad .$$

Here we assume the photino does not interact in the detector and that the parameters

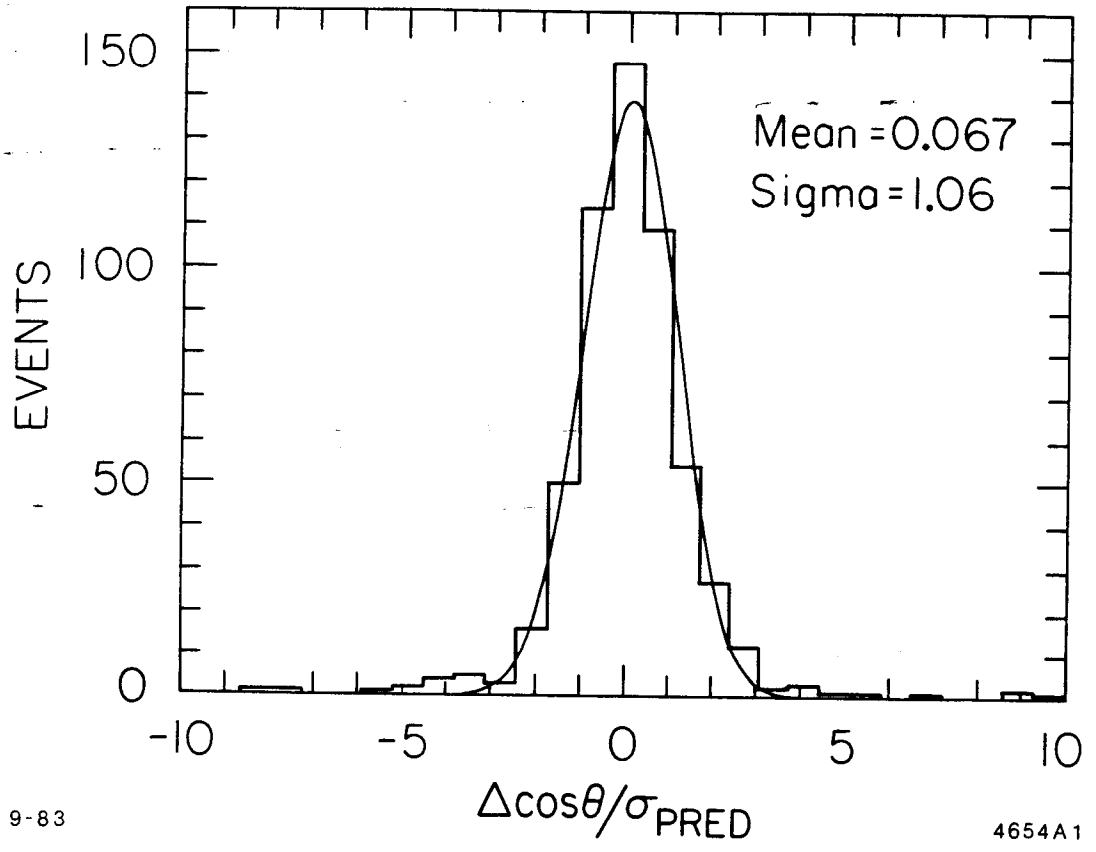

Fig. 18. Distribution of $(\cos\theta_{\text{predicted}} - \cos\theta_{\text{observed}})/\sigma_{\cos\theta}$ for events with one seen electron and one seen photon. The solid curve is the best fit to the data as described in the text.

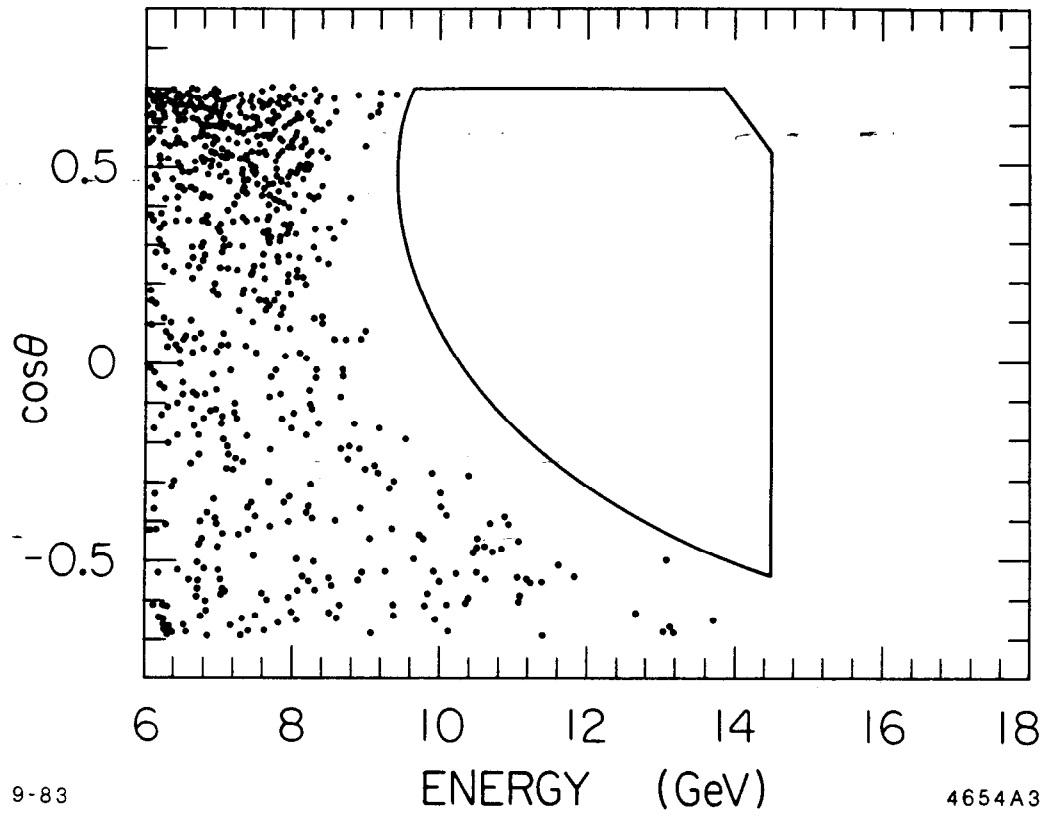

Fig. 19. MARK II acceptance for single negative prongs. Also shown is a scatter plot of single-prong events. Positive-charge prongs have $\cos\theta$ replaced by $-\cos\theta$.

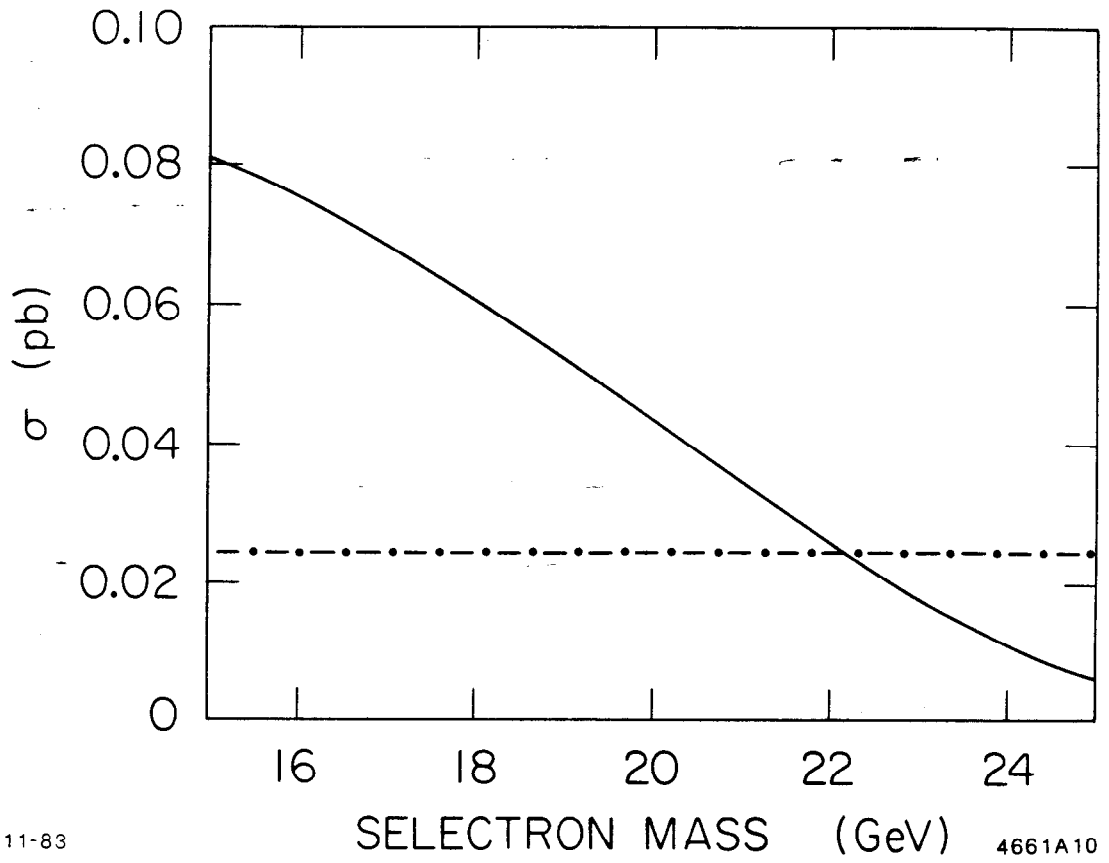

Fig. 20. Cross-section for singly produced selectrons as a function of selectron mass. The dot-dashed line is the 95% C.L. limit on single selectron production.

of right-handed and left-handed electrons are degenerate. If one partner is infinitely heavy, the mass limit for the lighter selection becomes 19.4 GeV/c^2. Both limits exceed previously published limits on the selectron mass.[34–36]

6. Weak Neutral Current Couplings of Leptons

The standard model[37] of Weinberg-Salam-Glashow unified the weak and electromagnetic interactions. In this model the differential cross sections for lepton pair production were sensitive to the interference between the weak neutral current and the electromagnetic current. The weak neutral current, mediated by the Z^0, was characterized by two dimensionless coupling constants g_a (axial vector) and g_v (vector). The model predicts $g_a = -1/2$ and relates g_v to the weak mixing angle, $g_v = 2\sin^2\theta_W - 1/2$. We report a high statistics measurement of the differential cross sections for the reactions:

$$e^+e^- \rightarrow e^+e^- \qquad \text{(Reaction 1)}$$

$$e^+e^- \rightarrow \mu^+\mu^- \qquad \text{(Reaction 2)}$$

$$e^+e^- \rightarrow \tau^+\tau^- \qquad \text{(Reaction 3)}$$

based on a data sample corresponding to an integrated luminosity of 100 pb^{-1}.

The unpolarized relativistic cross section for Reactions (2) and (3), including Z^0 exchange, is

$$\frac{4s}{\alpha^2}\frac{d\sigma}{d\Omega} = (1+\cos^2\theta)\left(1 + \frac{G_F g_v^e g_v^\ell}{\pi\alpha\sqrt{2}}\,\frac{sM_z^2}{s-M_z^2}\right) + \left(\frac{2G_F g_a^e g_a^\ell}{\pi\alpha\sqrt{2}}\,\frac{sM_z^2}{s-M_z^2}\right)\cdot\cos\theta \qquad (7)$$

where G_F is the Fermi coupling constant, and θ is the angle between the outgoing positive lepton ℓ and the positron beam direction $\hat{z}$. Terms proportional to G_F arise from the interference between the weak and electromagnetic amplitudes. The axial vector component produces a forward-backward asymmetry in Reactions (2) and (3), and the vector component shifts their cross section relative to (1); both g_a and g_v modify the shape of the cross section in Reaction (1). The expression for Bhabha scattering is more complicated due to t–channel exchange diagrams.

The selection criteria for Reactions (1) and (2) yield 5312 μ pairs and 81309 Bhabha events. The more complicated decay topology of the tau gives 3714 events after all selection criteria are applied. Total background corrections of 0.03% ($e^+e^- \to \tau^+\tau^-$) and 2.9%±0.9% ($e^+e^- \to e^+e^-\mu^+\mu^-$, $\tau^+\tau^-$, hadrons) are applied to Reactions (1) and (2) respectively. Reaction (3) is corrected for contaminations of 1.6% from $e^+e^- \to \mu^+\mu^-(\gamma)$, 1.4% from hadronic backgrounds, and 3.1% from two-photon processes. The event acceptances at $\cos\theta = 0$ are 77%, 80% and 60% for Reactions (1), (2) and (3) respectively, and fall to 73%, 77% and 52% at $|\cos\theta| = 0.6$. The acceptance corrected, background subtracted, differential cross sections are shown in Figs. 21, 22 and 23 and are compared to $O(\alpha^3)$ QED prediction.

From uncertainties in the background estimates, errors in detector simulation and uncertainty in the decay modes of the tau, we find a 1.6% normalization error on the ratio $\sigma_{\mu\mu}/\sigma_{ee}$ and a 2.8% error on the ratio $\sigma_{\tau\tau}/\sigma_{ee}$.

We use a maximum likelihood technique to fit Reactions (1)–(3) to the $O(\alpha^3)$ QED cross section plus the weak contributions[38] using the corrected $\cos\theta$ distributions. Setting $g_v^2 = 0$, we find $g_a^e g_a^\mu = .32 \pm .07 \pm .02$ and $g_a^e g_a^\tau = .19 \pm .09 \pm .02$, where the first error is statistical and the second systematic. The fits yield acceptance, background, and QED corrected forward-backward electroweak asymmetries, extrapolated to full $\cos\theta$ interval, of $A_\mu^{weak} = -7.1\% \pm 1.7\%$ and $A_\tau^{weak} = -4.2\% \pm 2.0\%$ where the standard model predicts $A^{weak} = -5.7\%$, radiatively corrected.[39] The fitted cross sections are superimposed on the data in Figs. 22 and 23. The $\mu - \tau$ universality of the axial-vector current is tested and we find $g_a^\tau/g_a^\mu = 0.6 \pm 0.3$. If we assume $e-\mu-\tau$ universality $g_a^2 = .27 \pm .06 \pm .02$ from Reactions (2) and (3). From a simultaneous fit to all three reactions we find $g_a^2 = .23 \pm .05 \pm .02$ and $g_v^2 = .03 \pm .03 \pm .03$, where systematic errors have been explicitly included in the fit and the fitted cross section is superimposed on the data in Fig. 23. Table II[40] summarizes e^+e^- data on g_v^2 and g_a^2 and gives a world average.

These results are in good agreement with the standard model. The probability that QED alone would have led to the results presented here is 6×10^{-7}. The weak couplings were computed in the limit $M_Z \to \infty$. For a $M_Z \sim 93$ GeV/c^2,[41] and including radiative corrections, g_a^2 is only decreased by 2.5%.

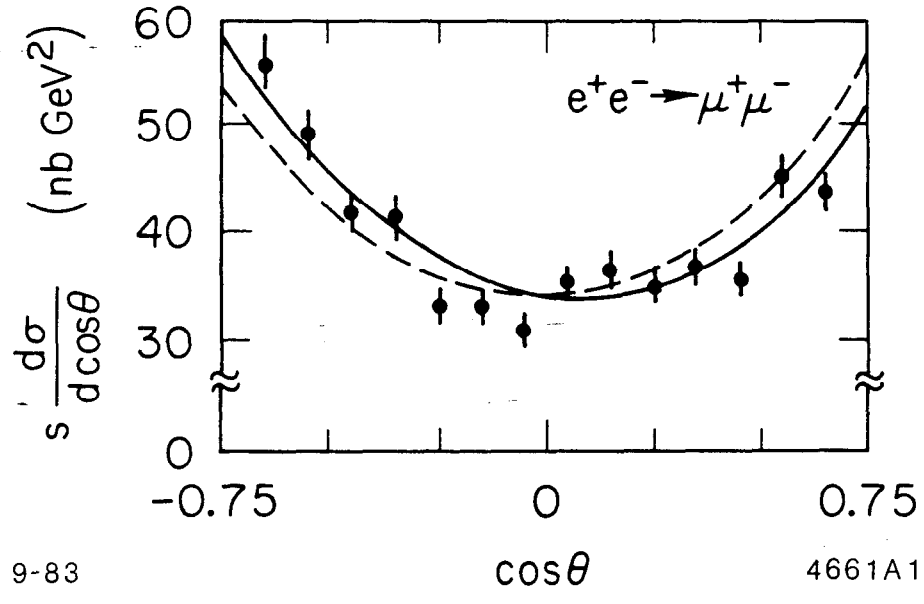

Fig. 21. The differential cross sections for Reaction (2), normalized to the QED prediction are shown. The dashed line corresponds to the $O(\alpha^3)$ QED cross section and the solid line to the fitted cross section.

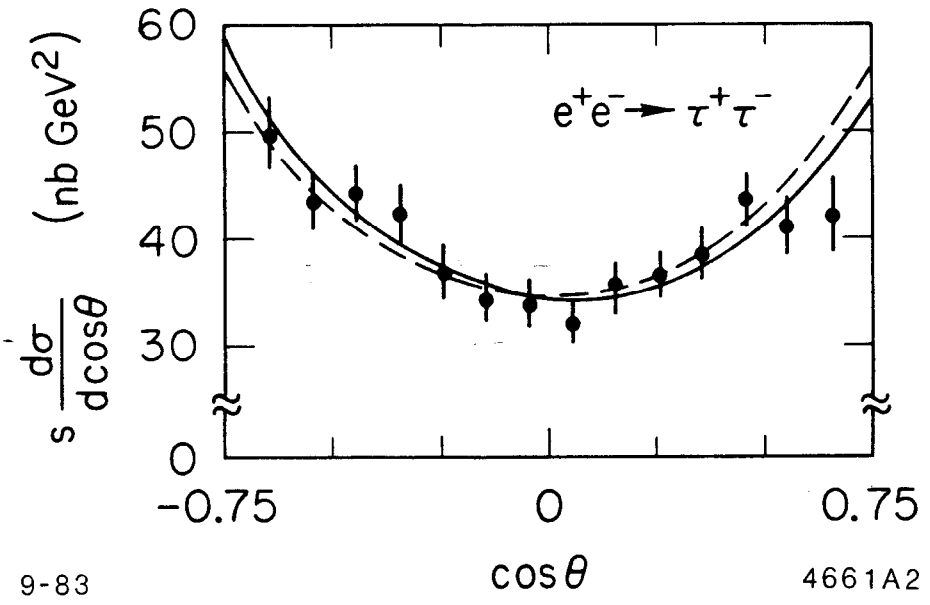

Fig. 22. The differential cross sections for Reaction (3), normalized to the QED prediction are shown. The dashed line corresponds to the $O(\alpha^3)$ QED cross section and the solid line to the fitted cross section.

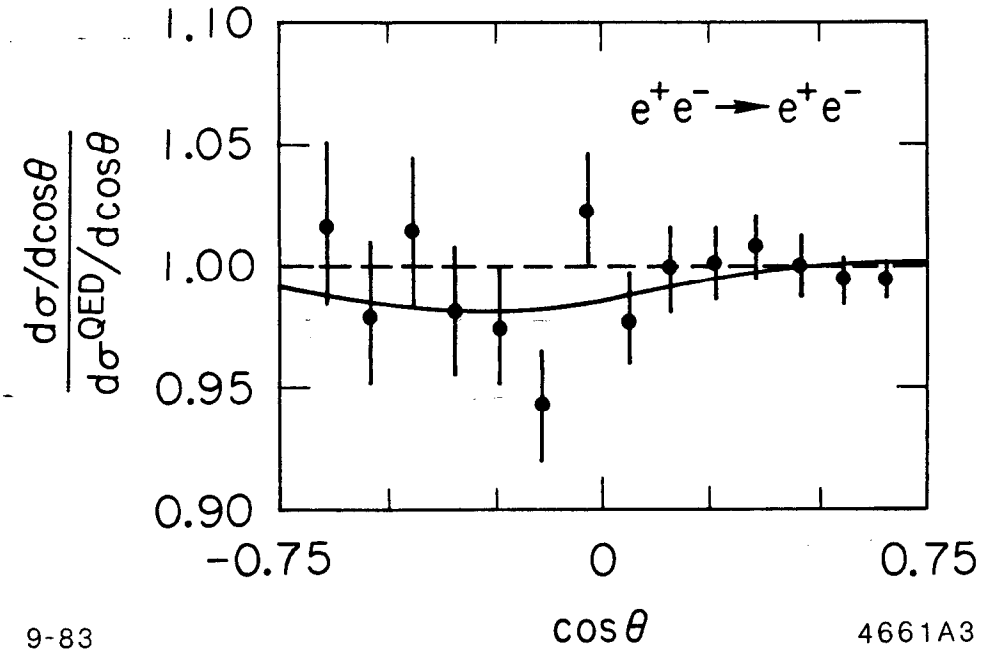

Fig. 23. This is the ratio of the differential cross section for Reaction (1) to the $O(\alpha^3)$ QED prediction. The experimental cross section is normalized to the electroweak cross section taken from a simultaneous fit to all three reactions. The dashed line corresponds to the $O(\alpha^3)$ QED cross section and the solid line to the fitted cross section.

Table II

Expt.	g_v^2	g_a^2
CELLO	$-.03 \pm .08$	$.30 \pm .12$
JADE	$.01 \pm .08$	$.30 \pm .05 \pm .03$
MAC	$.03 \pm .16$	$.24 \pm .04 \pm .01$
MARK II	$.03 \pm .03 \pm .03$	$.23 \pm .05 \pm .02$
MARK J	$.01 \pm .05 \pm .06$	$.31 \pm .04 \pm .03$
TASSO	$-.04 \pm .06$	$.24 \pm .06 \pm .01$
WORLD AVG.	$.005 \pm .03$	$.26 \pm .02$

If we assume $(g_a^e)^2 = 1/4$ from the standard model, take $g_v^2 = 0.0016$ ($\sin^2\theta_W = 0.23$) from neutrino scattering experiments, and set $M_Z = 93$ GeV/c^2, then we find the ratio of the measured to the expected cross section normalized to Bhabha events is $1.002 \pm .013 \pm .016$ in Reaction (2), and $0.996 \pm .016 \pm .028$ in Reactions (3) and extract the vector couplings $g_v^e g_v^\mu = .00 \pm .05 \pm .06$ and $g_v^e g_v^\tau = .01 \pm .06 \pm .09$. The coupling of the tau are summarized in Table III[42] and compared to world data.

Table III

Expt.	$g_v^e g_v^\tau$	$g_a^e g_a^\tau$
CELLO	$---$	$.28 \pm .14$
JADE	$---$	$.22 \pm .08$
MAC	$---$	$.06 \pm .13$
MARK II	$.01 \pm .06 \pm .09$	$.19 \pm .09 \pm .02$
MARK J	$---$	$.22 \pm .11$
TASSO	$< .55$	$.16 \pm .13$
WORLD AVG.		$.19 \pm .04$

A thorough description of this electroweak analysis can be found in Ref. 43.

7. Weak Neutral Current Couplings of the b Quark

We present a preliminary study of the angular distributions of events tagged with an energetic lepton in order to find evidence for the weak neutral current in the process

$$e^+e^- \to b\bar{b} \quad .$$

A very simple form of the angular distribution for the above process is given by

$$\frac{d\sigma}{d\cos\theta} = \frac{\pi\alpha^2 Q_b^2}{2s}\left[(1+\cos^2\theta) - \frac{4g_a^e g_a^b \chi}{\alpha Q_b}\cos\theta\right] \tag{8}$$

where χ is a constant related to the Fermi coupling G_F, the square of the center-of-mass energy s and M_Z. Here Q_b is the charge of the bottom quark, $-1/3$, g_a^b is the axial vector coupling of the b quark and θ is the polar angle between the quark and the incoming electron.

We study the b quark couplings because bottom events are relatively easy to tag using leptons and we expect a large forward-backward asymmetry at $\sqrt{s} = 29$ GeV of

$$A_b = -0.19$$

with a full solid angle detector. However the reality of the measurement is there exists no clean sample of bottom events and the low tagging efficiency reduces the statistics compared to $e^+e^- \to \mu^+\mu^-$ by over an order of magnitude.

The technique is quite straightforward. A b-enriched, c-enriched and background sample of events are assembled using the lepton tagging technique described in Section 2. The sign of the quark comes from the sign of the lepton. Therefore

$$b \to e^- \quad \bar{b} \to e^+ \qquad \text{and} \qquad c \to e^+ \quad \bar{c} \to e^- \quad .$$

However, the b-enriched sample contains $c\bar{c}$ events, leptons from the cascade decay $b \to c \to \ell$, and nonprompt sources of leptons. These effects and others either cancel or dilute the signal we are trying to measure.

We use a maximum likelihood technique to fit for g_a^b where we fix charm relative to bottom and take into account the fractions of each type of background and the

corresponding asymmetries of these backgrounds. The angular distributions for the three regions, b-enriched, c-enriched and background are shown in Figs. 24(a)-(c). The solid curves are the best fit solutions and the dashed curves are for the symmetrical case. From the fit, we find $g_a^b = -0.75 \pm^{0.35}_{0.30} \pm 0.20$ which can be compared to the Weinberg-Salam-Glashow value of $g_a^b = -1/2$. The above results are consistent with zero at a confidence level of only 2%.

8. K* Production

We have searched for evidence of the reaction $K^{*\pm} \to K^0_S \pi^\pm$ based on a data sample of hadronic events corresponding to an integrated luminosity of ~ 100 pb^{-1}. A preliminary analysis shows a clear signal for $E_{K^*} > 3.5$ GeV. This is shown in Fig. 25. We form the ratio of cross sections for K^* and K° and find

$$\frac{\sigma_{K^*}}{\sigma_{K^\circ}} = 0.84 \pm .17 \pm .25$$

for $E_{K^*,K} > 3.5$ GeV. This indicates a large vector fraction in the fragmentation process. Naively, we expect three vector particles for every one pseudo scalar, and hence a ratio of 0.75. Our results are consistent with data presented by the TPC (W. Hofmann) collaboration at this conference.

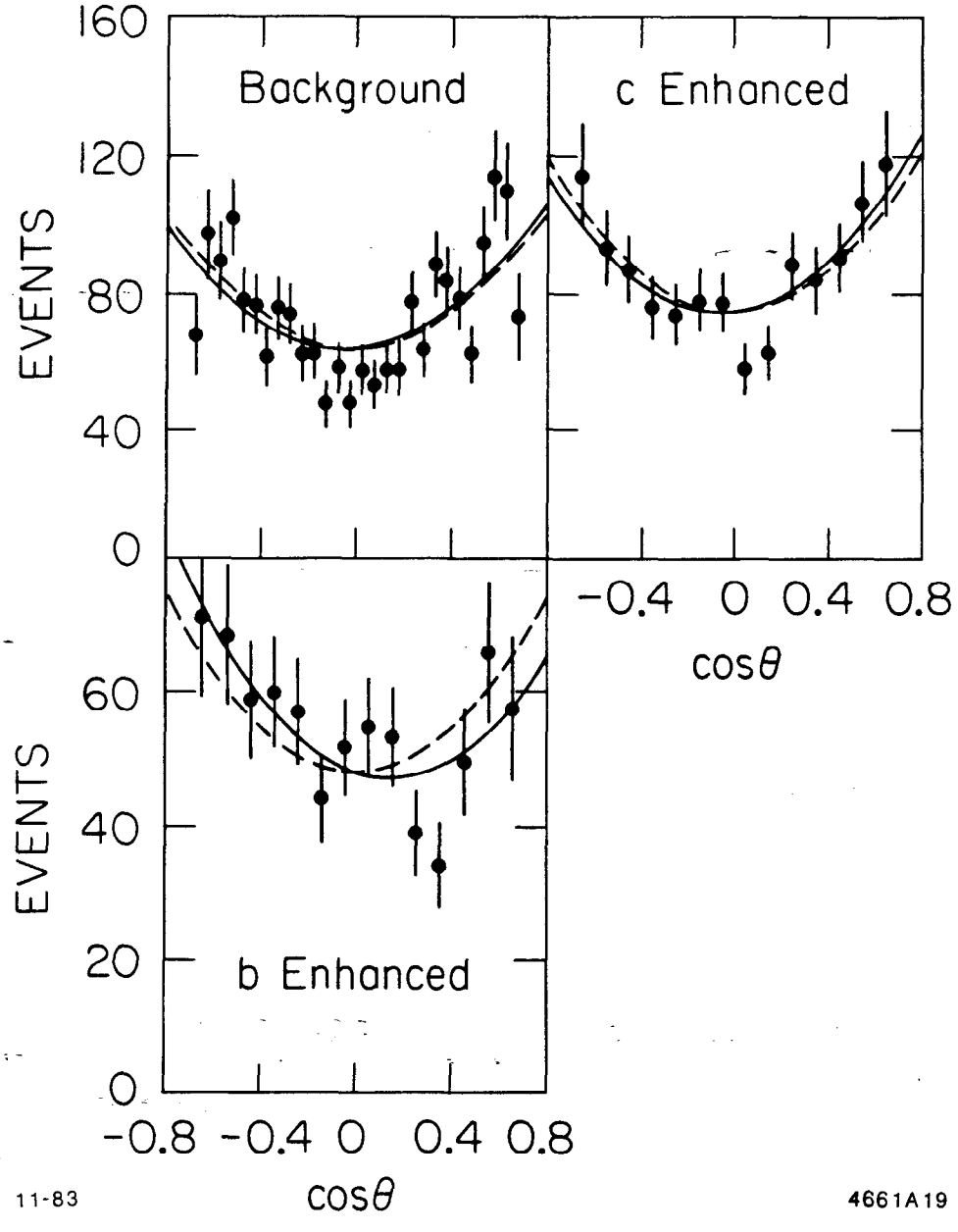

Fig. 24. Thrust angular distributions in the three regions. Dashed line is a symmetrical curve and solid curve is best fit to the data.

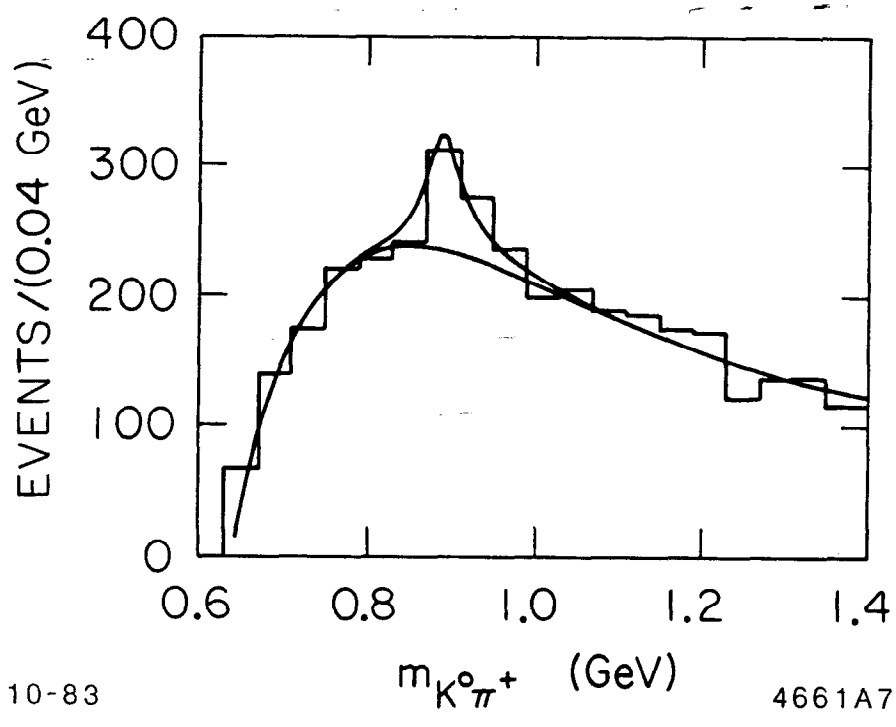

Fig. 25. $K_S\pi$ invariant mass distribution for $E_{K^+} > 3.5$ GeV. Curves show area fit to the background and K^*.

References

1. Members of the MARK II SLAC-LBL-Harvard Collaboration are: G. S. Abrams, D. Amidei, A. R. Baden, C. A. Blocker, A. M. Boyarski, M. Breidenbach, P. Burchat, D. L. Burke, J. M. Dorfan, G. J. Feldman, G. Gidal, L. Gladney, M. S. Gold, G. Goldhaber, L. Golding, G. Hanson, D. Herrup, R. J. Hollebeek, W. R. Innes, J. A. Jaros, M. Jonker, I. Juricic, J. A. Kadyk, A. J. Lankford, R. R. Larsen, B. LeClaire, M. Levi, N. S. Lockyer, V. Lüth, C. Matteuzzi, M. E. Nelson, R. A. Ong, M. L. Perl, B. Richter, M. C. Ross, P. C. Rowson, T. Schaad, H. Schellman, D. Schlatter, R. F. Schwitters, P. D. Sheldon, J. Strait, G. H. Trilling, C. de la Vaissiere, J. M. Yelton and C. Zaiser.
2. R. Helm *et al.*, SLAC-PUB-3070 (1983).
3. J. A. Jaros, in *Proceedings of the International Conference on Instrumentation for Colliding Beam Physics*, SLAC-Report 250, edited by W. Ash, Stanford, California (1982).
4. J. Dorfan, SLAC-PUB-2813 (1981).
5. J. D. Bjorken, Phys. Rev. D17, 171 (1978); M. Suzuki, Phys. Lett. 71B, 139 (1977).
6. N. Abramowicz *et al.*, Z. Phys. C15, 19 (1982).
7. W. B. Atwood, SLAC-PUB-2980, 1982.
8. M. E. Nelson *et al.*, Phys. Rev. Lett. 50, 1542 (1983).
9. M. J. Puhala *et al.*, Phys. Rev. D25, 695 (1982).
10. R. D. Field and R. P. Feynman, Nucl. Phys. B136, 1 (1978).
11. A. Ali *et al.*, Phys. Lett. 39B, 155 (1980).
12. W. Bacino *et al.*, Phys. Rev. Lett. 43, 1073 (1979).
13. E. Thorndike, talk presented at XVIII Rencontre de Moriond (CLEO), March (1983); P. M. Tuts, talk presented at XVIII Rencontre de Moriond (CUSB), March (1983).
14. C. Peterson *et al.*, Phys. Rev. D27, 105 (1983).
15. D. Schlatter, SLAC-PUB-2982, 1982.

16. See talks at this Conference by R. Ehrlich (CLEO), J. Lee-Franzini (CUSB), C. Young (DELCO), M. Piccolo (MAC), E. Lohrmann (PETRA Review).

17. M. E. Nelson, Ph.D. Thesis, LBL-16724 (1983).

18. M. Kobayashi and T. Maskawa, Prog. Theor. Phys. 49, 652 (1973). For a recent review of quark mixing angles see Ling-Lie Chau, Phys. Rep. 95, (1983).

19. P. Ginsparg and M. Wise, HUTP-83/A027 (1983); E. Paschos, B. Stech and U. Türke, CERN-TH-3601 (1983).

20. P. Ginsparg, S. Glashow and M. Wise, Phys. Rev. Lett. 50, 1415 (1983).

21. E. Fernandez *et al.*, Phys. Rev. Lett. 51, 1022 (1983); N. S. Lockyer *et al.*, Phys. Rev. Lett. 51, 1316 (1983).

22. M. Gaillard and L. Maiani, in *Proceedings of the 1979 Cargese Summer Institute on Quarks and Leptons*, ed. by M. Levy *et al.*, Plenum Press, New York, 1979, p. 433.

23. F. J. Gilman and J. S. Hagelin, Phys. Lett. 126B, 111 (1983); and SLAC-PUB-3226 (1983).

24. B. Winstein *et al.*, Fermilab proposal 617.

25. See for example M. Wirbel, Phys. Lett. 121B, 252 (1983).

26. G. J. Feldman *et al.*, Phys. Rev. Lett. 48, 66 (1982).

27. W. T. Ford *et al.*, Phys. Rev. Lett. 49, 106 91982).

28. H. J. Behrend *et al.*, Nucl. Phys. B211, 369 (1983).

29. C. A. Blocker *et al.*, Phys. Lett. 109B, 119 (1982). The uncertainty in τ_τ comes primarily from the error in B_e.

30. J. M. Yelton *et al.*, Phys. Rev. Lett. 49, 430 (1982).

31. P. Fayet and S. Ferrara, Phys. Rep. 32C, 249 (1977).

32. E. Witten, Nucl. Phys. B202, 253 (1982).

33. M. K. Gaillard, I. Hinchliffe and L. Hall, Phys. Lett. 116B, 279 (1982); Phys. Lett. Errata, to be published.

34. H. J. Behrend *et al.*, Phys. Lett. 114B, 287 (1982).

35. R. Brandelik *et al.*, Phys. Lett. 117B, 365 (1982).

36. D. Cords, *Proceedings of the 20th International Conference on HEP*, Wisconsin, 1980, p. 590.

37. S. Glashow, Nucl. Phys. 22, 579 (1961); S. Weinberg, Phys. Rev. Lett. 19, 1264 (1967); A. Salam, in "Elementary Particle Theory," Proceedings of the 8th Nobel Symposium, ed. by N. Svartholm (Almquvist and Wiksells, Stockholm, 1968), p. 367.

38. R. Budny, Phys. Lett. 45B, 340 (1973); Phys. Lett. 55B, 227 (1975).

39. F. A. Berends, R. Kleiss and S. Jadach, Nucl. Phys. B202, 63 (1982).

40. H. J. Behrend *et al.*, Z. Phys. C16, 301 (1983). W. Bartel *et al.*, Phys. Lett. 108B, 140 (1982). Phys. Lett. 99B, 281 (1981). E. Fernandez *et al.*, Phys. Rev. Lett. 50, 1238 (1983). B. Adeva *et al.*, Phys. Rev. Lett. 48, 1701 (1982). R. Brandelik *et al.*, Phys. Lett. 117B, 365 (1982). B. Naroska, invited talk presented at the International Symposium on Lepton and Photon Interactions at High Energies, Ithaca, New York (1983).

41. G. Arnison *et al.*, Phys. Lett. 126B, 398 (1983). P. Bagnaia *et al.*, Phys. Lett. 129B, 130 (1983).

42. H. J. Behrend *et al.*, Phys. Lett. 114B, 282 (1982). B. Naroska, invited talk presented at the International Symposium on Lepton and Photon Interactions at High Energies, Ithaca, New York (1983).

43. M. Levi *et al.*, Phys. Rev. Lett. 51, 1941 (1983).